DR. CONCHA ARENAS (Orcid ID : 0000-0002-4212-0524)

Article type : Original Manuscript

Lacustrine stromatolites: Useful structures for environmental interpretation – an example from the Miocene Ebro Basin

LETICIA MARTIN-BELLO*, CONCHA ARENAS* and BRIAN JONES†

**Division of Stratigraphy, Department of Earth Sciences, Geotransfer Group and Institute for Research on Environmental Sciences of Aragón (IUCA), University of Zaragoza. 50009 Zaragoza, Spain.* (E-mail: leticia.martin.bello@gmail.com)

†*Department of Earth and Atmospheric Sciences, University of Alberta. Edmonton, Alberta T6G 2E3, Canada*

Associate Editor – Alexander Brasier

Short Title – Lacustrine stromatolites, Ebro Basin

This article has been accepted for publication and undergone full peer review but has not been through the copyediting, typesetting, pagination and proofreading process, which may lead to differences between this version and the Version of Record. Please cite this article as doi: 10.1111/sed.12577

ABSTRACT

The significance of stromatolites as depositional environmental indicators and the underlying causes of lamination in the lacustrine realm are poorly understood. Stromatolites in a *ca* 600 m thick Miocene succession in the Ebro Basin are good candidates to shed light on these issues because they are intimately related to other lacustrine carbonate and sulphate facies, grew under variable environmental conditions and show distinct lamination patterns. These stromatolites are associated with wave-related, clastic-carbonate laminated limestones. Both facies consist of calcite and variable amounts of dolomite. Thin planar stromatolites (up to 10 cm thick and less than 6 m long) occurred in very shallow water. These stromatolites represented first biological colonization after: (i) subaerial exposure in the palustrine environment (i.e. at the beginning of deepening cycles); or (ii) erosion due to surge action, then coating very irregular surfaces on laminated limestones (i.e. through shallowing or deepening cycles). Sometimes they are associated with evaporative pumping. Stratiform stromatolites (10 to 30 cm high and tens of metres long) and domed stromatolites (10 to 30 cm high and long) developed in deeper settings, between the surge periods that produced hummocky cross-stratification and horizontal lamination offshore. Changes in stromatolite lamina shape, and thus in the growth forms through time, can be attributed to changes in water depth, whereas variations in lamina continuity are linked to water energy and sediment supply. Growth of the stromatolites resulted from *in situ* calcite precipitation and capture of minor amounts of fine-grained carbonate particles. Based on texture, four types of simple laminae are distinguished. The simple micrite and microsparite laminae can be grouped into light and dark composite laminae, which represent, respectively, high and low Precipitation/Evaporation ratio periods. Different lamination patterns provide new ideas for the interpretation of microbial laminations as a function of variations in climate-dependent parameters (primarily the Precipitation/Evaporation ratio) over variable timescales.

Keywords Environmental indicators, lacustrine stromatolites, lamination patterns, morphogenesis factors, saline carbonates, storm and fair-weather conditions.

INTRODUCTION

Microbial laminated deposits/structures are common in many marine (Park, 1976; Riding, 2000; Reid et al., 2003; Tang et al., 2014) and continental (Casanova, 1994; Linqvist, 1994; Cohen et al., 1997; Zamarreño et al., 1997) carbonate successions. Depositional and hydrological interpretations on the distribution of stromatolites have commonly been based on the external and internal geometric attributes of the stromatolites (Reid et al., 2003; Andres & Reid, 2006; Arenas & Pomar, 2010; Jahnert & Collins, 2011; Bosak et al., 2013a, b; Awramik & Buccheim, 2015; Tosti & Riding, 2017). Although the environmental significance (for example, water depth, current velocity, salinity, sediment distribution) of stromatolites in marine realms is generally understood (Reid & Browne, 1991; Jahnert & Collins, 2012, 2013; Mercedes-Martín et al., 2014), the relationships between stromatolites and other sedimentary facies in lacustrine systems is still open to debate (e.g. Awramik & Buchheim, 2009; Noffke & Awramik, 2013; Renaut et al., 2013). With the exception of the studies by Awramik & Buchheim (2009), Bouton et al. (2016), Létteron et al. (2018) and Vennin et al. (2018), stromatolites in saline lacustrine environments have received little attention. In particular, stromatolites and associated facies in lakes subject to temporal variations in water levels and repetitious surge activity merit detailed sedimentological analyses in order that their impact on stromatolite growth, at all scales, can be assessed.

The Miocene lacustrine succession in the north-central part of the Ebro Basin of north-east Spain, which is up to *ca* 600 m thick and well-exposed over a vast area (Fig. 1), includes numerous beds that are formed of well-preserved stromatolites (Figs 2 and 3). There, the spatial and temporal relationships of the stromatolites to their associated lacustrine carbonate and sulphate facies are clearly evident. This succession provides the basis for this study, which focuses on the: (i) depositional setting of the stromatolites in the lacustrine depositional cycles; (ii) environmental parameters, such as water energy and depth, and sediment supply, that controlled stromatolite morphogenesis; and (iii) internal architecture of the stromatolites (i.e. textures and lamina arrangements).

The main aims of this study are to: (i) describe the external morphology of the stromatolites and their associated facies in order to delineate the spatial distribution of the stromatolites relative to fluctuations in the lake level; (ii) fully characterize internal growth forms and lamina shape in the stromatolites so that the processes involved in their formation (storms, fair-weather conditions, sediment supply and water level variations) can be accurately inferred; and (iii) analyse the different types of laminae based on their texture and cyclic arrangement so that the temporal durations and controlling climate parameters can be reasonably inferred.

Critically, this research shows that: (i) stromatolite development was commonly the first biological colonization after subaerial exposure and/or subaqueous and subaerial erosional processes; and (ii) the internal architecture of the stromatolites reflects climate-dependent parameters over variable timescales. In so doing, this study provides new information regarding the development of lacustrine stromatolites. They involve the proposal of models that explain the depositional environment and the internal architecture through different time and space scales and incorporate approximate temporal durations for the lamination patterns. The relations between lamina attributes, internal growth forms, discontinuities and erosional features are set within the frame of depth versus water energy and sediment supply. These proposals provide a basis for the interpretations of depositional conditions and lamina-forming processes of other stromatolite-bearing sequences.

STRATIGRAPHIC AND GEOLOGICAL CONTEXT

The Ebro Basin, an Alpine basin in the northeast part of the Iberian Peninsula bounded by the Pyrenean, Iberian and Catalonial coastal ranges (Fig. 1A), is usually considered the southernmost foreland basin of the Pyrenees. There, the Palaeocene to Miocene sedimentary succession is divided into eight tectosedimentary units (T1 to T8; ., 2002; Pardo et al. 2004) that include marine and continental deposits. From the Early Oligocene to the Middle Miocene, the basin was an endorheic area that became filled with alluvial and fluvial sediments derived from the Pyrenean,

Iberian and Catalonial ranges. These detrital sediments graded laterally into sulphate and carbonate lacustrine sediments in the basin centre. In the Middle or Late Miocene, drainage was towards the Mediterranean Sea. The phase of erosion that followed continues to the present day (García-Castellanos et al., 2003; Vázquez-Urbez et al., 2013). During the Pliocene and Quaternary, extensive erosion sculpted several uplands in the central part of the basin. The Sierra de Alcubierre, which is the focus of this study, is one of those uplands where strata are horizontal or dip at a low angle to the south.

In the Sierra de Alcubierre, the conformable tectosedimentary units T5, T6 and T7 are well-exposed (Figs 1B and 2). These units, which span from the Ramblian to the Aragonian (Burdigalian–Serravallian) (Muñoz et al., 2002), have recently been dated precisely by magnetostratigraphic studies (Pérez Rivarés et al., 2002; Pérez Rivarés, 2016). Unit T5 (Figs 1B and 3) comprises 350 m of gypsum, marls, limestones and dolostones that grade laterally into limestones and marls to the east and north. Further north, these lacustrine deposits pass laterally into fluvial mudstones and sandstones (Fig. 2). Unit T6 (Figs 1B and 3), up to 135 m thick, is formed largely of limestones and marls that include interbeds of gypsum towards the south-west. Unit T7 (Figs 1B and 3) includes 110 m of mudstones, sandstones, limestones and marlstones. This is a portion from the complete record of T7, which is found only in the western part of the basin (Muñoz et al., 2002; Pérez Rivarés, 2016). The terrigenous sediments in these three units of this area came from the Pyrenean region (Arenas et al., 1993). The stromatolites, which are the focus of this study, are composed mostly of calcite and less abundant dolomite. They are distributed throughout units T5, T6 and T7 (Figs 2 and 3).

SEDIMENTOLOGICAL FRAMEWORK

The sedimentological framework and facies scheme (Table 1) of the Miocene lacustrine and fluvial succession in the central part of the Ebro Basin was established by Arenas (1993) and Arenas & Pardo (1999). The facies are defined on the basis of lithology, sedimentary structures, pedogenetic

characteristics and biological components (Table 1; Fig. 4). Three complete facies associations (FA1 to FA3 in Fig. 2) are present in units T5, T6 and T7. Each association, 0.5 to 3.0 m thick, comprises a vertical facies succession that resulted from the superposition of laterally related environments due to progradation, aggradation and/or retrogradation processes caused by changes in lake level through time. The complete facies associations have been recognized in the field. Variants of these facies associations result from the absence of one or more facies (Arenas & Pardo, 1999).

1 Facies Association 1 (FA1): The complete succession comprises, in ascending order, trough cross-bedded sandstones (St) → ochre mudstones (Fo) → grey mudstones (Fg) → massive limestones (Lm) → bioturbated limestones (Lb). This association formed in distal-alluvial plain settings that were affected by expansion of carbonate lacustrine settings. This facies association, common in units T5 and T7, does not contain stromatolites (Fig. 2).

2 Facies Association 2 (FA2): The complete succession comprises, in ascending order, stromatolitic limestones (Ls) → laminated limestones (Ll) → marls (M) → laminated limestones (Ll) → stromatolitic limestones (Ls) → massive limestones (Lm) → bioturbated limestones (Lb), that formed in carbonate lacustrine settings that became progressively deeper, with maximum depth represented by the marls, followed by shallowing. The stromatolites are always associated with the laminated limestones (Fig. 2). The complete FA2 is found in units T5 and T6, whereas only the shallowing upper part (Ll → Ls → Lm → Lb) is common in all of the units.

3 Facies Association 3 (FA3): The complete succession comprises, in ascending order, marls (M), grey mudstones (Fg), massive sandstones (Sm) → laminated gypsum (Gl), rippled gypsum (Gr) → lenticular gypsum (Glen) → laminated limestones (Ll), stromatolitic limestones (Ls) → nodular gypsum (Gn), that formed in shallowing sulphate lacustrine settings. Stromatolites, commonly associated with the laminated limestones, are rare in this facies association (Fig. 2): FA3 is common in unit T5 and locally at the base of unit T6, particularly on the southern side of the Sierra de Alcubierre.

The most complete FA2, found in units T5 and T6, represents a complex deepening–shallowing cycle, in which marls (M) correspond to the deepest part. Their deposition is linked to water inputs that led to the depth increase and lake expansion and supplied fine siliciclastic sediment. The laminated and stromatolitic facies represent carbonate deposition in shallower, more saline conditions during long periods of water residence in the lake and high evaporation, which is consistent with the previous stable isotope analyses of the carbonates (Table 2; Arenas & Pardo, 1999). At the same time, variable energy conditions are reflected by the sedimentary structures of the laminated limestones. Hummocky cross-stratification (HCS) corresponds to both tri-dimensional hummock and swaley morphologies and, more frequently, to megaripples, and can be up to 25 cm high and up to 2 m wide. Irregular cross-cutting surfaces, gutters and coarse sand-size and pebble-size intraclast deposits provide evidence of the erosion that took place. The massive and bioturbated facies at the end of FA2 represent lower salinities that reflect water dilution caused by the expansion of the freshwater lake. This is inferred from the lower stable isotopic values of the massive and bioturbated facies relative to the other facies (Arenas et al., 1997). Later drops in lake level caused widespread palustrine conditions. In FA2, the different types of stromatolites and the related laminated limestones and dolostones reflect variations in energy and water levels, both in the shallowing (M $\rightarrow$ Ll $\rightarrow$ Ls $\rightarrow$ Lm $\rightarrow$ Lb) and deepening (Ls $\rightarrow$ Ll $\rightarrow$ M) parts of the cycle. Facies Association 3 (Fig. 2) represents sulphate environments, in which thin stromatolites and laminated limestones developed during phases of freshwater influx.

Arenas & Pardo (1999) and Arenas et al. (1999) developed a depositional model whereby high lake levels led to freshwater carbonate deposition with massive and bioturbated limestones and marls dominating (for example, in FA1 and FA2; Fig. 2). Conversely, low-lake levels led to the development of playa-lake environments where sulphate and halite facies developed (for example, in FA3; Fig. 2). The stromatolites and laminated limestones developed during the oscillations from high to low lake levels, when saline carbonate lake conditions existed.

METHODS AND MATERIALS

This study is based on the stratigraphic and sedimentological analyses of eight sections that include stromatolites in units T5, T6 and T7 of the Miocene succession in the Sierra de Alcubierre (Figs 1 and 3) with the primary focus being on those parts of the sequence that contained stromatolites. One hundred and eighty-three samples were collected with most being stromatolites. Polished sections, small and large thin sections, and X-ray diffraction analyses (XRD) were produced from these samples. These, together with the analyses provided by Arenas (1993), were used for the structural, textural and mineralogical characterization of the carbonate deposits in the study area.

Field observations focused largely on their geometry and spatial relationships with other facies. One hundred and twelve polished slabs and 147 thin sections were used to study the textures and general structures of the stromatolites. In this work, the term *micrite* is used for calcite crystals <4 μm long, whereas dolomicrite is formed of dolomite crystals <4 μm ng . *Microsparite* refers to calcite crys s h r 4 10 μ m ng nd *sparite* is used for crystals >10 μm (cf. T ck r & Wrigh , 1990; Verrecchia et al., 1995; James & Jones, 2015). Fifty-two samples were ground and sieved (62 μm) for XRD analyses on a D-Max Rigaku diffractometer (Rigaku, Tokyo, Japan) equipped with a graphite monochromator and CuKa radiation at the *Servicio de Apoyo a la Investigación (*SAI) at the University of Zaragoza. Twenty-two samples (each *ca* 10 mm x 10 mm) were studied using scanning electron microscopy (SEM) with energy dispersive X-ray spectroscopy (EDS) at the University of Alberta (Zeiss Sigma 300 VP-FESEM/EDS; Zeiss AG, Oberkochen, Germany) and the University of Z r g (C r Z i ss ER LIN™ FESE ; Zeiss AG, Oberkochen, Germany), operating at 3 to 15 kV and 158 pA.

Seventy samples (one sample per lamina) were taken from the calcite stromatolites of units T5 (2 specimens; 37 laminae) and T6 (3 specimens; 33 laminae) for isotopic analyses ($\delta^{13}C$ and $\delta^{18}O$). These analyses were undertaken so that the environmental interpretation of the different types of laminae could be deduced. Only specimens formed solely of calcite were sampled. Powdered samples were obtained on polished slabs using a micro-drill of 0.4 mm diameter (Navfram N120 Micromotor

25 000 rpm with electronic speed regulator). The isotopic analyses were done at the *Serveis científico-tècnics* of the University of Barcelona (Spain) using a Thermo Finnigan MAT-252 mass spectrometer (Thermo Fisher Scientific, Waltham, MA, USA) following standard procedures (Craig, 1965). The is pi c r s s r xpr s s d i n δ‰ VPDB (Vienna Pee Dee Belemnite) calibrated with international reference scales using the IAEA Certified Reference Material NBS-19. The error margin is ±0.04 for the $\delta^{13}C$ and ±0.12 for the $\delta^{18}O$.

MACROSCOPIC FEATURES OF STROMATOLITES AND ONCOLITES

The stromatolites, which are most common in units T5 and T6 (Figs 1 and 2), are typically associated with the laminated limestones. In general, these stromatolites developed during relatively uniform growth periods and are characterized by relative continuity of lamination through time. The descriptions of external morphology, internal growth forms and lamina shape follow the descriptive classification of Arenas et al. (1993) which is based largely on the terms defined in Kennard & Burne (1989) (Fig. 5).

External geometry and internal growth forms of stromatolites and oncolites.

The external geometry of stromatolites is described by their length to height ratio (L:H) and their shape. Based on external geometry observed in the field (outcrop scale; Fig. 6A to E), the stromatolites are divided into: (i) thin planar stromatolites; (ii) stratiform stromatolites; and (iii) domed stromatolites (Figs 6 and 7). Oncolites (Lo) are present locally (Fig. 7A). These terms are applied to individual stromatolites. Several individual stromatolites are commonly found adjacent to each other in the same layer.

Thin planar stromatolites (Ls.1)

The thin planar stromatolites (Ls.1) have greater lateral extent than height (1 mm to 10 cm thick, generally <2 m long but locally up to 6 m long), commonly have a L:H ratio of <60. They are characterized by smooth, flat to undulatory, laterally continuous laminae. These stromatolites can occur on regular to irregular substrates with the initial morphology of the stromatolite reflecting the morphology of the underlying surface. In most cases, the thin planar stromatolites consist of a single stromatolite body. In some examples, these stromatolites alternate with cm-thick beds of intraclast packstones and rudstones of laminated limestones with ripples (Ll.1; Table 1; Fig. 6E). The thin planar stromatolites are divided into types 1a, 1b and 1c according to the morphology of their lamina.

- Ls.1a, up to 5 cm thick, are characterized by flat, laterally continuous smooth laminae (Figs 6D, 6E and 7B).
- Ls.1b, up to 10 cm thick, are formed of gently undulating, laterally continuous smooth laminae; locally the laminae form conspicuous isolated, conical or semicircular domes (Figs 6D, 7C and 7D).
- Ls.1c, up to 10 cm thick, are formed of strongly undulating and convex-up laminae, with semicircular to semielliptical shapes in vertical cross section, forming small domes and non-branching columns (Figs 6A and 7E). The columns are linked laterally with variable inter-columnar space. In plan view, the columns are circular to elliptical, the latter with their long axes parallel to each other. In a few examples, enveloping laminae entirely overlap the underlying laminae (Fig. 5), with overturned lamina margins. They give rise to individual low-synoptic relief (Fig. 5), irregular, semielliptical domes (Fig. 7E) that are set adjacent to one another. These stromatolites are rooted on packstones and rudstones that are composed of intraclast, some of them being stromatolite fragments, and the spaces between them are occupied by marls and laminated limestones.

Stratiform stromatolites (Ls.2)

The stratiform stromatolites, 10 cm to 30 cm high and 10 to 30 m long, with a L:H ratio >>100 (Fig. 6E), are tabular or gently domed. They typically occur above the thin planar stromatolites and are always laterally and vertically related to laminated limestones. The stratiform stromatolites can, in some cases, be correlated over distances of 8 km. The stratiform stromatolites are formed of several internal growth forms (Fig. 5): domes, columns, and undulatory-laminated to flat-laminated forms of variable dimensions. Commonly, stromatolites have a slightly undulatory, laterally continuous growth form at the base (2 to 5 cm thick) that is overlain by columnar and domed internal growth forms (5 to 20 cm thick), though the opposite arrangement also exists. The domes and columns are commonly linked to one another by bridges, but some remain isolated (Fig. 7F) and generally show no preferential orientation in plan view (Fig. 6C). In columns and domes, with increasing width upwards, the laminae are usually highly enveloping (Figs 5 and 7F to H) and involve laminae with overturned margins (Figs 5 and 7E). Laminated limestones, including packstones and rudstones composed of intraclast, and marls, occupy the spaces between domes and columns (Fig. 7G and H; see Fig.15C and D below).

Domed stromatolites (Ls.3)

The domed stromatolites, 10 to 30 cm high, with a L:H of <1.5, are laterally related to the stratiform stromatolites and the laminated limestones (commonly Ll.2, with HCS) (Fig. 6B). The spaces between the individual stromatolites are of variable dimensions and are occupied by deposits of laminated limestones (Ll.2 and Ll.3). The internal growth forms of these stromatolites are the same as those of the stratiform stromatolites (Fig. 7F).

Oncolites (Lo)

Rare oncolites, 3 to 6 cm in diameter, are found at the base of some stratiform and domed stromatolites forming the nucleus of stromatolite growth (Fig. 7A). The elliptical oncolites are characterized by symmetric and/or asymmetrical coatings (0.5 to 5.0 cm thick) that developed around nuclei formed of marlstone or laminated limestone-dolostone fragments. The laminae are smooth. Small oncolites tend to have a symmetrical growth pattern whereas the larger oncolites have asymmetrical growth in the younger laminae.

Lateral and vertical relations of the stromatolites: facies associations (FA)

Based on the morphologies of the stromatolites and their position in the shallowing and deepening cycles, four variants of FA2 are recognized (Fig. 8A to D).

Stromatolites in deepening cycles, FA2-A (Fig. 8A and B).

There are two situations that occur in this case:

1 Stromatolites at the base of deepening cycles, FA2-A (Fig. 8A). Thin planar stromatolites occur on top of bioturbated limestones (Figs 6A and 7D); the latter are characterized by subaerial exposure features. These upper surface features are represented by very intense bioturbation (root marks and nodulization) (Fig. 4E and F), desiccation cracks, Fe-rich oxidized surfaces and centimetre to decimetre wide scours. Rip-up clasts with flatten oval and very irregular shapes (0.2 to 0.5 mm long) from the underlying limestones (bioturbated facies) and with laminar shape (0.3 to 1.0 mm long) from older stromatolites are commonly incorporated into the basal parts of the stromatolites.

2 Stromatolites through deepening cycles, FA2-B (Fig. 8B). Layers formed of thin planar stromatolites and small domed stromatolites alternate with laminated limestones with HCS (Ll.2; Fig. 8B). Some of the stromatolites developed on erosional surfaces (Figs 6D and 7D) that can be up to several centimetres deep. Stromatolites coat them by mimicking the eroded substrate shapes. Erosional features are also visible in some of the stromatolites, as non-continuous laminae at the upper part and stromatolite fragments that are locally found in the spaces between the internal growth forms or form layers of stromatolite fragments.

Stromatolites in shallowing cycles (Fig. 8C and D)

There are two situations that occur in this case:

1 Thin planar stromatolites (Ls.1), stratiform stromatolites (Ls.3) or domed stromatolites (Ls.2) that either alternate with or are located at the top of laminated limestones with ripples (Ll.1) and parallel lamination (Ll.3; Fig. 8C), some being associated with nodular gypsum facies (Gn; Fig. 4A).

2 Thin planar stromatolites (Ls.1) followed by stratiform stromatolites (Ls.2) or domed stromatolites (Ls. 3; Fig. 8D), passing vertically into laminated limestones with parallel lamination (Ll.3) or with HCS (Ll.2, Fig. 6B), followed by massive (Lm) and bioturbated facies (Lb).

Distribution of stromatolites and oncolites through space and time

Thin planar stromatolites, stratiform and domed stromatolites occur in unit T5, with the best development being in the northern part of the Sierra de Alcubierre (sections VS, PL, PS, AL and LN; Fig. 1), where they are found in the deepening and shallowing portions of FA2 (Figs 2 and 8). In the southern part of the Sierra, gypsum facies are common in unit T5 (for example, sections BL, LF and

SC; Figs 1 and 2), and only a few thin planar stromatolites and domed stromatolites are found in section LF (Fig. 1). In this section, most stromatolites are found in the shallowing portion of FA2-C (Figs 6A and 8C) and less commonly in FA3.

In unit T6, thin planar stromatolites, stratiform and domed stromatolites are also present, with the best development being on the south side of the Sierra (i.e. sections BL, LF and SC sections), where they are found in FA2 (Fig. 8). The occurrence of charophyte (thali) fragments, ooids and sparite crystal laminae in or associated with the stromatolites is most common at the base of unit T6, both in the north and east (sections PS and LN) and in the south of the Sierra (sections BL and SC). Unit T7 only contains thin planar stromatolites as part of shallowing, commonly incomplete, FA2-C (Fig. 8). Rare oncolites are present at the base of some domed stromatolites and stratiform stromatolites in units T5 and T6.

TYPES OF LAMINAE AND LAMINATION PATTERNS IN THE STROMATOLITES

Following Walter (1972) and Preiss (1972), who defined a *lamina* as: " h s m s n i f y r ing", a *single lamina* is herein defined as a layer that is <10 mm thick, has a uniform texture, and is separated from underlying and overlying laminae by boundaries that denote sharp to gradual changes in colour and/or texture (cf. Arenas & Jones, 2017; Fig. 9A). Two or more simple laminae can be grouped into a *composite lamina* (Arenas et al., 2015; Arenas & Jones, 2017). Each composite lamina is distinguished from the underlying and overlying composite or simple laminae by changes in thickness, colour and/or texture (Fig. 9B). The composite laminae can be formed of the same type or different types of simple laminae. The stromatolites from Sierra de Alcubierre are formed largely of micrite, dolomicrite, microsparite (Figs 9 and 10A to C) and scattered patches of sparite (Fig. 10D and E). As such, they are fine-grained or micritic stromatolites *sensu* Riding (2000).

The stromatolite laminae are always smooth, with variable cross-sectional shapes ranging from flat, to undulatory, to gently to steeply convex (Figs 5, 9 and 10). Lateral changes in thickness characterize many laminae. The stromatolites are formed of simple laminae that can be grouped into two different types of composite laminae: dark composite laminae and light composite laminae (Fig. 11A and B).

Simple laminae (Fig. 11A)

Four types of simple laminae are defined based on their texture, colour and/or porosity (Figs 9, 10 and 11A).

1 *Dark dense micrite laminae (DD)*. These laminae, 0.04 to 0.5 mm thick (mean *ca* 0.1 mm; N = 45) (Figs 9A and 10C), are composed of dark grey micrite, and usually darker towards the top (Fig. 9B). Their thickness is generally uniform, and they have gradual or sharp bases and sharp tops. The micrite is formed of densely packed subhedral to anhedral calcite crystals. Rare pores, up to 40 μm long, commonly filled with subhedral calcite crystals, are typically aligned parallel to bedding. These laminae contain scattered spherulitic bodies that are <10 μm in diameter.

2 *Light porous/clotted micrite to microsparite laminae (LP).* These laminae, 0.1 to 1.3 mm thick (mean *ca* 0.4 mm; N = 79) (Figs 9A, 9B, 10A and 10C), are formed of light grey to light brown to yellow porous micrite and microsparite. Their thickness varies laterally, increasing at the summits of the domes and thinning downward and locally disappearing (Fig. 10A), and they typically display clotted to clotted-micropeloidal fabrics, with clots <50 (10 to 20) μm in diameter (Figs 10C and 11D). Porosity usually increases towards the top of the laminae. The pores (0.1 to 0.3 mm wide) are irregular, some being elliptical with their long axes perpendicular to lamination. Some are filled with subhedral microsparite or microcrystalline gypsum crystals. Scattered spherulites, *ca* 10 μm in diameter, are present in some laminae.

3 *Light dense micrite laminae (LD).* These laminae, 0.1 to 1.9 mm thick (mean *ca* 0.7 mm; N = 42) (Fig. 10F and G), are formed of light grey or light brown to yellow micrite. Their thickness varies laterally. These laminae pass gradually upward into light porous/clotted micrite to microsparite laminae (Fig. 10F and G). Disperse, small (0.1 to 0.5 mm) quartz grains and clay minerals are present with bioclasts (mollusc, ostracod and charophyte fragments), intraclasts (including stromatolite fragments) and ooids (0.12 to 0.75 mm diameter) (Fig. 10D and F). These components are commonly aligned parallel to bedding. The light dense laminae are formed of anhedral to subhedral calcite and dolomite crystals that are 1 to 5 μm long.

3 *Fibrous laminae.* These laminae, 0.01 to 0.3 mm thick (mean *ca* 0.1 mm; N = 15), commonly alternate with the micrite laminae (both the porous and dark dense laminae). The constituent sparite crystals have their long axes perpendicular to lamination (Fig. 10E and H). The continuity of the fibrous laminae is variable, and lateral changes to dense micrite are common (Fig. 10E). Fibrous laminae are conspicuous in the summit of some domes and columns. The fibrous laminae are commonly found in stromatolites that contain allochemical grains (ooids, intraclasts and bioclasts; Fig. 10D) and siliciclastics that are scattered within or aligned parallel to light dense micrite laminae. Some coated grains include fibrous laminae.

Composite laminae (Fig. 11B)

The simple micrite and microsparite laminae can be grouped into two types of composite laminae (Figs 9B, 10B and 11B).

1 *Dark composite laminae (DCL),* from 0.3 to 2.8 mm thick (mean *ca* 1.2 mm; N = 43), that are formed of: (i) dark, dense micrite laminae that include intercalated, thinner light porous/clotted micrite to microsparite laminae (DCL1); or (ii) successive dark dense micrite laminae (DCL2). They are formed of 2 to 30 simple laminae (Fig. 10B).

2 *Light composite laminae (LCL),* from 0.6 to 6.4 mm thick (mean *ca* 2.4 mm; N = 32). They are formed of: (i) a thick light porous lamina with thin dense dark simple lamina intercalated (LCL1); or (ii) an alternation of porous and light dense laminae (LCL2; Figs 10B and 11B).

Lamination patterns

Based on the terms established by Monty (1976), three patterns of laminations are evident in the stromatolites in the study area (Fig. 11C to H).

1 *Simple alternating lamination*. Alternating dark dense and light porous simple laminae (Fig. 11D).

2 *Cyclothemic lamination*. Succession of cycles, each consisting of a light dense lamina at the base, followed by a light porous simple lamina and a dark dense simple lamina at the top (Fig. 11E).

3 *Composite alternating lamination*. Alternating dark composite laminae and light, either simple or composite, laminae. The dark composite laminae can be both DCL1 and DCL2. The light laminae can be both LCL1 and LCL2, and also a simple light porous lamina (Figs 9B, 10B, 10F and 11F to H).

The stromatolites are composed of one or more types of the above lamination patterns (Fig. 11C). In the latter case, the thickness of each type of lamination varies through space and time in the same stromatolite.

Microbial structures in the dark and light laminae

Evidence of microbes is not obvious. Arenas et al. (1993) also noted the rarity of microbial filaments in the stromatolites of the Sierra de Alcubierre and concluded that 'coccoid b c ri ' were probably responsible for stromatolite formation. Although filamentous bodies attributable to microbes are present in some samples (for example, in samples from BL, PL, LF and SC sections; Fig. 12A and B), they are not ubiquitous. The dark dense and the light porous/clotted laminae contain loose structures or filament moulds (cf. Monty, 1976), 0.2 to 1.0 mm long and 0.02 to 0.06 mm diameter, that are (sub)perpendicular to the bedding formed of micrite or sparite (Fig. 12A) and resemble filamentous microbes. In some cases, the clotted-peloidal micrite in the light porous/clotted laminae delineate elongate structures, up to 0.5 mm long and 0.01 mm thick, that are perpendicular or subperpendicular to lamination (Fig. 12B). Some light porous/clotted laminae encompass convex-up or fan-like shapes, up to 1 mm high, consisting of radially set filamentous bodies (Fig. 12C). These bodies probably represent filamentous cyanobacteria that grew in small colonies.

STABLE ISOTOPE ANALYSES

The isotopic analyses from consecutive laminae mostly correspond to composite dark (N = 34) and composite light laminae (N = 36) (Table S1). The alternation of both types of laminae shows cyclic variations of the isotopic values in the five analysed specimens (Fig. 13). In each of them, the light laminae have lower $\delta^{13}C$ and $\delta^{18}O$ values than the dark laminae. Individual and mean values of samples in each specimen are provided in Table S1.

INTERPRETATION: DEPOSITIONAL ENVIRONMENTAL CONDITIONS

Stromatolites through space and time

The distribution of stromatolites through space in units T5 and T6 is consistent with growth in a shallow, low-gradient, saline carbonate lake. The lake received most water and sediment input from the north, and experienced extensive shoreline migrations (Arenas & Pardo, 1998, 1999). During deposition of unit T5, most of the stromatolites formed as a fringe in the northern areas of the Sierra de Alcubierre, close to the shoreline. During deposition of unit T6, which corresponded to an overall dilution of the carbonate lake (Figs 2 and 3), saline carbonate conditions were restricted to the more southern areas during periods when lake levels were lower. Unit T7 contains only a few thin planar stromatolites associated with laminated limestones with ripples in shallowing FA2-C and FA2-D (Fig. 8). These two facies encompass numerous ooids. In this lake context, the sparite-dominated texture is favoured by humid conditions (cf. Casanova, 1994; Freytet & Verrecchia, 2002). This is consistent with overall deposition conditions inferred for unit T7, i.e. progradation of a Pyrenean fluvial system, migration of lake shoreline southward and occurrence of inter-channel ponds (Arenas & Pardo, 2000).

Significance of the stromatolites and oncolites in the lacustrine system

The occurrence of the microbial mats and their external morphologies varied as a function of water depth and energy conditions (Fig. 8) in the saline carbonate lake environment where the stromatolites formed. Stromatolites at the base of the deepening cycles (Figs 2 and 8A) represent the first microbial colonization after prolonged subaerial exposure in the palustrine environment (Figs 4E, 4F and 6A). The fact that stromatolites are the first facies that developed on top of bioturbated facies (i.e. with root traces and nodulization) indicates that they developed in shallow and/or marginal lake areas. The formation of stromatolite fragments and *in situ* erosion of some stromatolites resulted from erosion that took place: (i) in very shallow to subaerial conditions, denounced by ripples and cracks on the stromatolite surfaces; and (ii) under subaqueous conditions, from wave surge action associated with storms during the formation of laminated limestones with ripples or with HCS (Fig. 14A and B). The

thin planar stromatolites and the overlying domed stromatolites developed in response to an increase in water depth, and consequent lake expansion. Laminated limestones with HCS suggests a relative depth increase associated with periods of storm-induced waves (cf. Duke, 1985; Haines, 1988). Subsequent laminated limestones with parallel lamination corresponds to offshore deposition by storm-induced density currents after surge action (Fig. 14B). Marls higher in the sequence (for example, in Fig. 8A) reflect increased deepening, linked to surface water inputs into the lake and, thus, also represent lacustrine expansion.

Most of the thin planar stromatolites that alternate with the laminated limestones with parallel lamination represent shallow, calm water conditions (Fig. 8C and D). Laminated limestones with ripples and with parallel lamination formed as a result of sheet flows generated by water inputs that generated deposits in marginal, shallow lake areas (cf. Eyles & Clark, 1986). The stromatolites developed between periods when shore sheet flows and surges were active (Fig. 14A and C). This notion is supported by the stromatolite fragments that were formed during the higher energy periods (Fig. 15). The development of thin planar stromatolites and small domed stromatolites at the top of the laminated limestones (Fig. 8C) took place in shallow water and were prone to subaerial exposure. This inference is supported by the occurrence of gypsum nodules in the stromatolites. These nodules formed through evaporative pumping associated with shallow water or exposure of the areas where the stromatolites were growing (Figs 4A, 6A and 8C). In contrast, the domed stromatolites and stratiform stromatolites developed as the water became deeper (cf. Awramik & Buchheim, 2015; Roche et al., 2018). Higher water level and fair-weather conditions promoted vertical growth of the domed stromatolites and stratiform stromatolites. The continuous vertical growth of the stromatolite laminae and the lack of erosive features in the stromatolites are consistent with this interpretation. The vertical and lateral association of stromatolites with laminated limestones with HCS and with parallel lamination (Fig. 8B and D) suggests variable energy conditions (Fig. 15A and B) caused by storms that disturbed the normal fair-weather conditions (cf. Dumas & Arnott, 2006; Awramik & Buchheim, 2009). Storm surge caused partial breakage of some of the stromatolites that produced stromatolite fragments, which accumulated along the lake shore as laminae and between the columns and domes

within any type of stromatolites. Storm surge also produced various erosional features, such as irregular surfaces and gutters, on the substrate that were later coated by microbial mats (Fig. 15A and B).

The massive limestones and bioturbated limestones at the top of the shallowing FA2-D (Fig. 8D) formed as a result of the input of freshwater that caused water dilution, lake expansion and relative deepening (for example, WL1 in Fig. 14A). Later water level drop led to the expansion of the palustrine areas and subaerial exposure (cf. Arenas & Pardo, 1999).

To sum up, in the different situations in which stromatolites developed (Fig. 8), the stromatolites reflect relative changes in water depth and hydrodynamic conditions (Fig. 14). Taking into account the relationships between the stromatolites and the facies associated with them, and the lateral relationships between those and other lacustrine carbonate facies, a sedimentary facies model has been proposed for the Miocene stromatolite formation in the Sierra de Alcubierre (Fig. 14). Following exposure and/or erosion of the lake floor by storm surge and currents, microbial mats colonized the surfaces that were commonly irregular in morphology. Evidence of exposure and erosion is provided by intense bioturbation (Fig. 4E and F), desiccation cracks, Fe-rich oxidized surfaces and scours on bioturbated limestones, and irregular cross-cutting surfaces and gutters on laminated limestones. The stromatolite growth was, however, periodically interrupted by desiccation or by erosion caused by surge action associated with the formation of laminated limestones (for example, breakage; Fig. 15A and B). The thin planar stromatolites grew in shallow water conditions that occurred over large areas of the lake, which is supported by the lateral extension of this type in the field. The change from these stromatolites to stratiform or domed stromatolite, and the change from flat to convex-up growth forms reflect an increase in water depth. Rare oncolites that formed in shallow water commonly acted as nuclei for the growth of the domal and columnar stromatolites.

Internal structure of stromatolites: lamina shape, lamina arrangement and thickness variations

The three geometric types of stromatolites and the oncolites have the same textural features, lamina shape variations and lamina arrangement, which indicates that the same types of building microbes were responsible for all of them. If so, the changes of stromatolite morphology probably reflects changes in the physical parameters.

Irregular lateral changes in lamina thickness, in some cases involving thicker growth on the crests than in the valleys, are common features of many of the stromatolites (Fig. 10A, B and G). These thickness changes are better related to the variable microbial growth and concomitant grain trapping and calcification that reflect local conditions (for example, currents, water level, lightness or turbidity), as proposed by Hofmann (1973), Monty (1976) and Bosak et al. (2012, 2013a). The upper parts of the stromatolites (for example, crests of the domes and columns), for example, are the preferred loci for microbes due to higher light intensity, reduced abrasion, and a higher supply of fine-grained, suspended sediment (cf. Hand & Bartberger, 1988). Within individual stromatolites, changes in the lamina shape through time are as follows (Fig. 16A and B):

1 An upward change from slightly undulatory at the base, to increasingly convex laminae through time, forming domes and columns (Fig. 7C, F and G), that represent: (i) increasing water depth where laminae are continuous between the linked columns and domes (for example, Fig. 7C); or (ii) increasing water depth and higher energy levels if the laminae are discontinuous (i.e. in unlinked and bridged columns and domes; Fig. 15C).

2 An upward change from steep, multi-convex domes to gently convex to slightly undulate laminae upward (Fig. 7H) that developed as water depth decreased.

Herein, a proposed model for internal stromatolite morphogenesis is based on lamina shape, lamina continuity and internal growth forms of the stromatolites and their relation to associated facies (Fig. 16A and B). Domes and columns formed of laminae with dominant upright growth and high synoptic

relief (Figs 7C, 7G, 7H and 15C) developed during rising lake levels (cf. Andres & Reid, 2006). As level rise, the microbial growth, grain capture and concomitant mat calcification were enhanced, and the upright development took place as the stromatolites reacted to the change in lake level. This is consistent with the increased thickness of the light porous and light dense laminae towards the tops (Fig. 10A). In contrast, domes and flat semi-elliptical forms with their lower synoptic relief (Figs 7E, lower part of 7F and 14A) probably grew in stable, shallow water conditions. This type of asymmetrical development, which is very common over irregular substrates, probably represents water level close to, or at times slightly below, the top of the stromatolites, and perhaps without water between domes and columns during some periods.

The preferential growth direction is explained by some authors (Golubic, 1973) as a consequence of current direction. In this case, the random orientation of columns and domes (for example, Fig. 7F, lower part) means that is impossible to infer the preferential directions of water movement. Local environmental conditions greatly control column inclination (Hofmann, 1973). From all of the above facts, in the study case, the main control on the highly asymmetrical growth of stromatolites was water level.

Th ‘ nv pi ng’ nature of the laminae in many of the unlinked domes and columns (Fig. 15A and B) and the synoptic relief are indicators of minimum water depth (Fig. 16A) and of sediment supply to the inter-column and inter-dome spaces. Sediment supply must have been minimal when the enveloping laminae developed (for example, Figs 7G, 7H and 15A) because there is no evidence that sediment interfered with their growth. Moreover, in the discrete domes and columns, the dark laminae extend further down than the light laminae. The light laminae gradually wedge downward and eventually disappear and/or are covered by the dark laminae (Figs 7F, 7G and 15C). These features may imply that the light laminae formed under changing energy conditions whereas the dark laminae formed under stable water level. The lack of intraclasts or other grains within the dark laminae supports this interpretation.

Discontinuous growth of stromatolites and related erosional features

The laterally and vertically discontinuous laminae record a complex evolution of the microbial mats. The colonization and growth of the microbes was periodically interrupted by erosion caused by currents and waves. Subsequent deposition included filling of the inter-column and inter-dome spaces and of the spaces between the individual stromatolites with the sediments that compose the laminated limestones (with ripples and HCS and locally, coarse intraclasts and stromatolite fragments) (Fig. 15).

Several stages of microbial accretion and microbial interruption are evident in some stromatolites (Fig. 15A and B). In contrast, continuous lamination throughout the thin planar stromatolites and between the domes and columns in some of the domed stromatolites and stratiform stromatolites (Fig. 7C and E) are indicative of low-energy conditions (Fig. 16A and B).

Interruption of the stromatolite growth is indicated by features of different scales. These include erosional features in the stromatolites and inter-column spaces, and the presence of stromatolite fragments in the laminated limestones. The fragments commonly form packstones and rudstones or occur as isolated particles in the micrite of laminated limestones (Fig. 15C and D). The inter-dome and inter-column spaces thus were loci where the microbial mats were not so well developed (cf. Noffke & Awramik, 2013; Bosak et al., 2013b; Tosti & Riding, 2017).

In plan view, most of the domes and columns are irregular, but mostly rounded to elliptical in shape (Fig. 6C). There are, however, rare examples of elongate forms that are aligned parallel to one another (Ls.1b; Fig. 6C) and that probably grew in shallow water.

In the Miocene lake studied here, storm-surge return flow formed unidirectional currents. These currents produced scouring (gutters) and other erosional features – on a macroscopic scale – in the shallow marginal areas. At the same time, they transported detrital material toward inner lake areas, producing laminated limestones with parallel lamination offshore (Fig. 14). In this context, the irregular domes and columns, with enveloping laminae and dominant non-elongate shape of columns in plan view, indicate low-energy and relatively stable water level during microbial accretion, which

is not comparable to a context of continuous scouring between columns (Fig. 16A; cf. Tosti & Riding, 2017). The depositional scenario resembles some of the shallow Holocene lakes in the East African Rift (for example, Lake Bogoria; Casanova, 1986, 1994; Renaut et al., 2013), despite the different hydrological and tectonic context. In these Holocene lakes, stromatolites developed at intermediate lake levels between freshwater, deltaic inputs and saline alkaline water levels.

COMPARISON WITH OTHER LACUSTRINE MICROBIALITES

Compared with the marine stromatolite record, few studies have focused on stromatolites found in lacustrine systems. Exceptions include stromatolites found in some Cenozoic lacustrine basins, including those in the East African Rift, where Casanova (1986, 1994) and Cohen et al. (1997) described a variety of Late Miocene to Holocene examples. Other examples have been reported from the Miocene of New Zealand (Lindqvist, 1994), where they are associated with largely siliciclastic lake deposits, the Oligocene–Miocene of the French Central Massif (Bertrand-Sarfati et al., 1994; Roche et al., 2018) and the Eocene Green River Formation in Utah, USA (Awramik & Buchheim, 2015; Chidsey et al., 2015; Della Porta, 2015). Examples of Pre-Cenozoic lacustrine stromatolites are scant with the exception of studies from the Cretaceous of the Gyeongsang Basin in Korea (Woo, et al. 2004; Nehza et al., 2009) and the Cameros Basin in Spain (Suarez-Gonzalez et al., 2014), from the lower Cretaceous of the Codó Formation in Brazil (Bahniuk et al. 2015), from the Upper Jurassic–Lower Cretaceous of Wessex Basin in the UK (Gallois et al., 2018), from the Triassic of the Arnstadt Formation in Germany (Arp et al. 2005) and from the late Archean in Western Australia (Awramik & Buchheim, 2009).

There are some similarities between the Oligocene to Miocene lacustrine stromatolites found in the Limagne Basin (French Central Massif) and the stromatolites documented herein. Two main characteristics can offer analogues: (i) the external morphology distribution, described by Roche et al. (2018); and (ii) the lamina characteristics under microscope, studied by Bertrand-Sarfati et al. (1994)

and Roche et al. (2018) in the same area. The major differences between Limagne Basin and Ebro Basin stromatolites are related to the height of the domes, cones and coalescent columns. The stromatolites from the Limagne Basin are up to 6 m high, whereas the domed and stratiform stromatolites in the Ebro Basin are up to 30 cm high.

External morphologies, lake level and hydrodynamics

External morphologies have commonly been used as diagnostic features of water level variations (Casanova, 1994; Chidsey et al., 2015; Muniz & Bosence 2015; Vennin et al. 2018). In the Limagne Basin, the vertical transition from flat and cauliflower morphologies to domes, cones and coalescent columns, resulted from an increase of the water level (Roche et al., 2018). In the Ebro Basin, increases in water level are reflected by the upward change from flat laminated stromatolites to domed or stratiform stromatolites. As noted by Della Porta (2015), similar flat and low relief stromatolites are found in lake margins of recent lacustrine systems, including Lake Tanganyika (East African Rift), Pavilion Lake (Canada) and Lake Clifton and Marion Lake (Australia).

Cauliflower-like and dome-like morphologies (Roche et al., 2018), similar to the domed or stratiform stromatolites in the Ebro Basin, have highly enveloping laminae. These morphologies are interpreted to occur between flat (shallow) and cones and coalescent columns (deep) morphologies (Roche et al. 2018). In stromatolites from the Green River Formation in the Uinta Basin, the upward change to lower synoptic relief (Chidsey et al., 2015) is suggestive of shallowing processes. Collectively, the available information suggests that the highly enveloping laminae and high synoptic relief reflect deeper conditions (Fig. 16).

Roche et al. (2018) assumed that flat morphologies developed under lower energy conditions than the cauliflower-shaped stromatolites that have a higher content of peloids and ooids as a result of wave activity. In the Ebro Basin, thin planar stromatolites can be associated with erosional features, and their laminae can include disperse peloids and ooids. As for the domed and stratiform

stromatolites in the study area, they are not consistent with a ridge-runnel scenario with continuous scouring between columns (cf. Bosak et al., 2013b). Similarly, they do not they form high and elongated columns separated by narrow straight runnels, as has been described in Mesoproterozoic stromatolites in China (Tosti & Riding, 2017).

The lateral relation between domed stromatolites and laminated limestones, indicative of surge activity in the Ebro Basin, has also been recognized in the lacustrine stromatolites from Brazil (Muniz & Bosence, 2015). There, the domed stromatolites are laterally associated with coarse grainy facies forming cross and plane-parallel stratification and they are interpreted to have developed between fair-weather and storm-weather conditions.

Lamina characteristics

The composite and simple laminae and the lamination patterns evident in the Ebro stromatolites are also visible in some of the lacustrine stromatolites of other basins. The light and dark laminae in the Ebro stromatolites are, for example, equivalent to the clear and dark layers found in the stromatolites from the Limagne Basin (Bertrand-Sarfati et al. 1994). The cement-dominated microfabrics (Roche et al., 2018) found in some of the stromatolites from the Limagne Basin are similar to fibrous laminae found in the Ebro stromatolites. The composite dark dense laminae in the Ebro stromatolites are equivalent to the micrite-dominated laminated or columnar microfabric described by Roche et al. (2018).

The stromatolites from the Limagne Basin generally contain more well-preserved filamentous microbes than Ebro stromatolites. In the Limagne stromatolites, filamentous microbes are common in the upper parts of the cones and coalescent columns, but scarce in the flat and cauliflower stromatolites (Roche, et al. 2018). Although filamentous microbes are also scarce in the flat and cauliflower stromatolites from the Ebro Basin the reason for this is unknown.

DISCUSSION

The relation between the gross morphology of stromatolites and water depth is also evident in other lacustrine (e.g. Bertrand-Sarfati et al., 1994; Casanova, 1994; Zamarreño et al., 1997; Arenas et al., 2007; Roche et al. 2018) and marine successions (e.g. Andres & Reid, 2006; Jahnert & Collins, 2013; Mercedes-Martín et al., 2014; Tosti & Riding, 2017). Mathematical models that simulate stromatolite morphologies (e.g. Grotzinger & Rothman 1996; Grotzinger & Knoll, 1999) have focused on some aspects of microbial growth, but as pointed out by Reid et al. (2003) and Bosak et al. (2013a), they do not relate morphogenesis with specific depth or variability on the energy conditions, or with biological responses to such conditions. Based on the above-mentioned and other studies, parameters such as water level fluctuation, water energy and sediment supply, considered in this study to influence the stromatolite morphology, can be collectively considered important factors affecting lacustrine stromatolite geometries.

The changes in the shape and arrangement of laminae, through space and time, evident in many stromatolites, have generally been attributed to changes in water depth, water energy and/or sediment supply (Logan et al., 1964; Hofmann, 1973; Riding, 2000; Dupraz, et al., 2006; Jahnert & Collins, 2013). The possibility that biocenosis may influence laminae morphology (Grotzinger & Rothman, 1986; Grotzinger & Knoll, 1999; Dupraz, et al., 2006), is still open to debate. In the study area, for example, it is difficult to relate changes in lamina shape through time to different types of bacteria, because these changes did not involve variations in textural features of the laminae.

Microbialite accretion and factors controlling calcification of microbial mats

Tosti & Riding (2017), based on Mesoproterozoic stromatolites from China, found that the stromatolite columns have mainly non-enveloping laminae and frequent branching, and the fabrics in these low-relief stromatolite columns and in the intervening spaces are similar. These authors suggested that these features were consistent with a: "…low relative accretion rate and mats that

accreted mainly by trapping fine-grained particles rather than by in situ precipitation…". The low-relief to moderate-relief stromatolites from the Ebro Basin with their distinct textures and structures in the intervening sediments are different. The Ebro stromatolites contain little evidence of calcified microbes (Fig. 12) apart from scattered examples found in the dark dense and light porous laminae. Although there is some evidence that these features may have formed due to *in situ* precipitation processes, the textural variety of the laminae, the wide array of lamina arrangement and the dominant micrite texture suggest that this was not the dominant process in stromatolite growth.

Calcification of the microbial mat is mostly linked to the $CaCO_3$ saturation levels of the water (Merz-Preiß & Riding, 1999; Arp et al., 2001; Pentecost, 2005; Pedley et al., 2009; Jones & Peng, 2014). In general, higher levels of calcite saturation tend to favour rapid calcite precipitation and in many microbial deposits, the dense, fine-crystal layers reflect precipitation under warm conditions when temperature and CO_2 outgassing were highest (cf. Kano et al., 2007; Gradzinski, 2010; Arp et al., 2010; Manzo et al., 2012; Arenas et al., 2014). Thus, it is tentatively proposed that the calcification of the Miocene stromatolites in the Ebro Basin took place primarily during warm conditions. Moreover, heterotrophic decomposition of extracellular polymeric substances (EPS) below the productive part of the microbial mat favours HCO^{-3} and Ca-ion liberation (Dupraz et al., 2009; Arp et al., 2010; Decho et al., 2005), which increases the saturation level with respect to calcite and thus favours intra-calcite precipitation. Perhaps this process is enhanced when the development of microbial mats on surface slows down or decreases.

Significance of the types of laminae and lamination in the Ebro Basin Miocene lacustrine stromatolites

The 'regularity' of stromatolite lamina accretion is an intriguing issue because of the variety of processes involved and the uncertainty about the time span represented by the different types of laminae (Arenas & Jones, 2017). Most laminated microbialites encompass more than one style of lamination (Monty, 1976; Casanova, 1994; Arenas et al., 2007; Suárez-González et al., 2014) and

several cyclicity ranks (Lindqvist, 1994; Seong-Joo et al., 2000; Storrie-Lombardi & Awramik, 2006; Petryshyn et al., 2012; Arenas et al., 2015). In fine-grained stromatolites, the most common pattern is an alternation of light porous and dark dense laminae that has been recognized in many different depositional settings (Monty, 1976; Park, 1976; Bertrand-Sarfati et al., 1994; Zamarreño et al., 1997; Kano et al., 2007; Tang et al., 2014). In many ancient stromatolites and oncolites, this pattern has been variously attributed to changes in temperature, precipitation and/or evaporation (Casanova, 1994; Lindqvist, 1994; Woo et al., 2004; Arenas et al., 2007). The duration represented by each lamina-pair has generally been based on textural and geochemical evidence (Seong-Joo et al., 2000; Riding, 2000; Arenas et al., 2015). Although each pair of laminae is usually attributed to one year of growth (cf. Kano et al., 2007; Arp et al., 2010), other studies of present-day fluvial stromatolites have shown that several laminae can form in a few months, with both periodic and non-periodic changes in the magnitude of the environmental parameters that influence lamina formation (Gradzinski, 2010; Vázquez-Urbez et al., 2010; Arenas et al., 2014). Daily to pluriannual laminations have been found in stromatolites that grew in a wide variety of environments (Hofmann, 1973; Monty, 1976; Petryshyn et al., 2012; Okumura et al., 2013).

The porous laminae found in some stromatolites have been attributed to cooler temperature and/or rainy conditions, whereas the dense laminae have been linked to warmer and/or drier conditions (e.g. Casanova, 1986, 1994; Frantz et al., 2014). These textural changes are generally attributed to variations in microbial mat development and textural effects caused by changes in calcite saturation of the water (e.g. Janssen et al., 1999; Reid et al., 2000; Manzo et al., 2012; Arenas & Jones, 2017). In regions with strong seasonal contrasts in temperature and/or precipitation, these textural variations of the laminae are normally consistent with stable isotope variations. Casanova (1986, 1994), for example, considered the light and dark laminae in Holocene lacustrine stromatolites to have formed by seasonal changes in the Precipitation/Evaporation ratio that affected the lake water chemistry. Similarly, textural and $\delta^{18}O$ and $\delta^{13}C$ variations of the laminae in mid-Cretaceous lacustrine stromatolites that grew in semiarid to arid conditions have been attributed to local climatic conditions that caused temporal oscillations in lake salinity and productivity (Nezha et al., 2009). In

fluvial environments, cyclic $\delta^{18}O$ variations have generally been attributed to seasonal variations in temperature given that evaporation has little effect on isotope fractionation in this setting (Chafetz et al., 1991; Andrews & Brasier, 2005; Kano et al., 2007; Osácar et al., 2013, 2016).

Stable isotope analyses ($\delta^{13}C$ and $\delta^{18}O$) of successive laminae in two stratiform stromatolites, and three thin planar stromatolites in the Sierra de Alcubierre (Table S1; Fig. 13; Martin-Bello et al., 2017) show cyclic isotopic variations, with the light laminae having lower $\delta^{13}C$ and $\delta^{18}O$ values than the dark laminae (Fig. 13). Therefore, in the closed-basin example studied here, the light laminae would correspond to more humid conditions (i.e. rainy), with larger soil-derived CO_2 input, whereas the dark dense laminae would form in drier conditions (cf. Leng and Marshall, 2004; Arp et al., 2005; Martin-Bello et al., 2017).

The significance of fibrous laminae in terms of environmental conditions is poorly understood. The fibrous laminae are attributed to early diagenesis products (Freytet & Verrecchia, 1999), but can also be preserved primary textures (Grotzinger & Knoll, 1999). In the study area, fibrous textures are considered primary features and might be linked to occurrence of specific microbes, as suggested by Freytet and Verrecchia (1998), but there is not enough evidence to support this assumption in the studied case. Fan microfabrics in lacustrine stromatolites of the Green River Formation have been interpreted as formed by abiogenic precipitation in cooler and deeper conditions, compared with the alternating micrite laminae (Frantz et al., 2014). The fibrous laminae may then represent more humid conditions (as suggested by Peryt, 1983). This environmental context is consistent with the common occurrence of fibrous laminae in unit T7 deposits, which overall deposited during wetter climate periods respect to the underlying units T5 and T6 (Arenas et al., 1997).

Integration of all available information indicates that different laminae developed at different times of the year in response to seasonal changes in conditions. Thus, the following cycles are evident:

- The light dense laminae with scattered allochems developed during the rainy season as freshwater was added to the lake (Figs 10F and 11A)
- The light porous laminae developed during the spring-summer period when higher temperatures promoted microbial growth (cf. Pentecost, 2005),
- The dense micrite laminae (Fig. 11A) were produced in the summer as evaporation increased.

It is possible that the winter records may be under-represented if the temperature was <10ºC and carbonate production ceased (Matsuoka et al., 2001; Brasier et al., 2010; Osácar et al., 2013; Arenas et al., 2018).

Rhythmic and cyclothemic laminations (Fig. 11C) in the stromatolites might reflect yearly cycles. Therefore, the various composite lamination patterns (Fig. 11C) represent complex variations through longer periods (for example, pluriannual variations), each governed by either dry or humid conditions (Fig. 17). For example, some dark composite laminae can reflect pluriannual periods of dominant dry conditions (low Precipitation/Evaporation ratio). Frantz et al. (2014), based on high-resolution chemical analyses, proposed decadal changes in the Precipitation/Evaporation ratio to explain textural variations in Eocene stromatolites of the Green River Formation. These temporal interpretations must, however, be taken as tentative proposals because some environmental parameters can change over shorter time spans, so that intra-seasonal laminae may also occur (Arenas & Jones, 2017). Further studies based on high resolution stable isotope and periodicity analyses of lamination will help refine the lamination patterns and their relation to climatic parameters in the Miocene sequence of the Ebro Basin.

CONCLUSIONS

Stratigraphic and detailed sedimentological analyses of stromatolites in Miocene lacustrine and distal alluvial sequences of the Ebro Basin explains how climate and depositional environmental conditions impacted their geometry, internal structure and texture at various temporal and spatial scales. These

stromatolites and the associated laminated limestones consist of calcite and less common dolomite and formed during oscillations between high water levels (freshwater carbonate deposition) and low water levels (sulphate deposition). The following conclusions relevant to the utility of stromatolites as indicators of environmental conditions can be highlighted:

1 Three different morphological types of individual stromatolites (i.e. thin planar stromatolites, domed stromatolites and stratiform stromatolites) selectively occurred at the beginning of or through deepening cycles, and through or at the top of shallowing cycles experienced by the lacustrine carbonate-depositing settings. Thus, they reflect changes in water depth and concomitant salinity.

2 Stromatolites grew in shallow lake fringes at periods of fair-weather conditions. Surge activity during storms interrupted their development and caused their partial erosion on different scales.

3 Stromatolites are typically the first deposits on disturbed areas, such as surfaces affected by prolonged subaerial exposure and/or erosional processes. In such conditions, microbial mats are pioneers in colonizing harsh habitats, for example, saline and very shallow water.

4 Changes in lamina shape and lamina arrangement within the stromatolites (i.e. variations of growth forms through time) reflect primarily water depth variations, whereas lamina continuity through space and time within the undulatory-laminated to flat-laminated growth forms, and between the domes and columns in the domed stromatolites and the stratiform stromatolites reflect changes in water energy (i.e. through shear) and sediment supply.

5 The different types of simple laminae (dark dense micrite, light porous micrite and microsparite, light dense micrite and fibrous calcite) and composite laminae record variations in the magnitude of climate-related parameters, primarily the Precipitation/Evaporation ratio and temperature, that likely affected the saturation state of water respect to calcite and the accretion processes. Cyclic variations in $\delta^{13}C$ and $\delta^{18}O$ of the light and dark laminae support such assumptions.

6 *In situ* calcite precipitation and minor capture of suspended fine-calcite particles may have accounted for the textural changes between laminae.

7 Rhythmic and cyclothemic laminations may reflect yearly cycles in Precipitation/Evaporation ratio, and the various composite lamination patterns pluriannual variations in that ratio.

ACKNOWLEDGEMENTS

This study was funded by project CGL2013-42867-P and FPI contract BES-2014-069389 of the Spanish Government and European Regional Funds. The results form part of the activities of the Geotransfer scientific group (Aragón Government, Operating Program FEDER Aragón 2014-2020). The Scanning Electron Microscopy, Optical Microscopy, and Rock Preparation services of the University of Zaragoza, Spain (Servicios de Apoyo a la Investigación) and the Scanning Electron Microscopy service of the University of Edmonton, Canada, are thanked for technical support. Dr. Ana María Alonso Zarza is kindly thanked for supervision. We are grateful to editor Dr. Alexander Brasier and anonymous reviewers for their critical reviews.

REFERENCES

Andres, M.S. and **Reid, R.P.** (2006) Growth morphologies of modern marine stromatolites: A case study from Highborne Cay, Bahamas. *Sed. Geol.*, **185**, 319–328. Available at: https://doi.org/10.1016/j.sedgeo.2005.12.020

Andrews, J. E. and **Brasier, A.T.** (2005) Seasonal records of climatic change in annually laminated tufas: Short review and future prospects. *J. Quatern. Sci.*, **20**, 411–421. Available at: https://doi.org/10.1002/jqs.942

Arenas, C. (1993) Sedimentología y paleogeografía del Terciario del margen pirenaico y sector central de la Cuenca del Ebro (zona aragonesa occidental). PhD thesis, University of Zaragoza, Zaragoza, 858 pp. Available at: https://zaguan.unizar.es/record/70725

Arenas, C. and **Jones, B.** (2017) Temporal and environmental significance of microbial lamination: Insights from Recent fluvial stromatolites in the River Piedra, Spain. *Sedimentology*. **64**, 1597–1629. Available at: https://doi.org/10.1111/ijlh.12426

Arenas, C. and **Pardo, G.** (1998) Storm carbonate deposits in Miocene lacustrine systems of the central Ebro Basin (north- eastern Spain). *Extended Abstracts AAPG Annual Convention*, Salt Lake City, USA, 1 (A-30), 1–3.

Arenas, C. and **Pardo, G.** (1999) Latest Oligocene-Late Miocene lacustrine systems of the north-central part of the Ebro Basin (Spain): Sedimentary facies model and palaeogeographic synthesis. *Palaeogeogr. Palaeoclimatol. Palaeoecol.*, **151**, 127–148. Available at: https://doi.org/10.1016/S0031-0182(99)00025-5

Arenas, C. and **Pardo, G.** (2000) Neogene lacustrine deposits of the north- central Ebro Basin, north-eastern Spain. In: *Lake Basins Through Space and Time* (Eds E.H. Gierlowski-Kordesch and K.R. Kelts). *AAPG Stud. Geol.*, 46, 395–406.

Arenas, C. and **Pomar, L.** (2010) Microbial deposits in upper Miocene carbonates, Mallorca, Spain.

Palaeogeogr. Palaeoclimatol. Palaeoecol., **297**, 465–485. Available at: https://doi.org/10.1016/j.palaeo.2010.08.030

Arenas, C., Auqué, L., Osácar, C., Sancho, C., Lozano, M.V., Vázquez-Urbez, M. and **Pardo, G.** (2015) Current tufa sedimentation in a high discharge river: A comparison with other synchronous tufa records in the Iberian Range (Spain). *Sed. Geol.*, **325**, 132–157. Available at: https://doi.org/10.1016/j.sedgeo.2015.05.007

Arenas, C., Alonso-Zarza, A.M. and **Pardo, G.** (1999) Dedolomitization and other early diagenetic processes in Miocene lacustrine deposits, Ebro basin (Spain). *Sed. Geol.*, **125**, 23–45.

Arenas, C., Cabrera, L. and **Ramos, E.** (2007) Sedimentology of tufa facies and continental microbialites from the Palaeogene of Mallorca Island (Spain). *Sed. Geol.,* **197**, 1–27. Available at: https://doi.org/10.1016/j.sedgeo.2006.08.009

Arenas, C., Casanova, J. and **Pardo, G.** (1997) Stable isotope characterization of the Miocene lacustrine systems of Los Monegros (Ebro Basin, Spain): palaeogeographic and palaeoclimatic implications. *Palaeogeogr. Palaeoclimatol. Palaeoecol.*, **128**, 133–155.

Arenas, C., Osácar, C., Auqué, L., Andrews, J.E., Pardo, G., Marca, A., Martín-Bello, L. and **Pérez-Rivarés, F.J.** (2018) Seasonal temperatures from $\delta^{18}O$ in Recent Spanish tufa stromatolites: Equilibrium redux!. *Sedimentology*, **65**, 1611–1630. Available at: doi:10.1111/sed.12440

Arenas, C., Pardo, G. and **Casanova, J.** (1993) Bacterial stromatolites in lacustrine Miocene deposits of the Ebro Absin (Aragon, Spain). In: *Studies on Fossil Benthic Algae.* (Eds F. Barattolo, P. De Castro and M. Parente), *Boll. Soc. Paleont. Ital. Spec. Vol*., 1, 9–22.

Arenas, C., Vázquez-Urbez, M., Auqué, L., Sancho, C., Osácar, C. and **Pardo, G.** (2014) Intrinsic and extrinsic controls of spatial and temporal variations in modern fluvial tufa sedimentation: A thirteen-year record from a semi-arid environment. *Sedimentology*, **61**, 90–132. Available at: https://doi.org/10.1111/sed.12045

Arp, G., Wedemeyer, N. and **Reitner, J.** (2001) Fluvial tufa formation in a hard-water creek (Deinschwanger Bach, Franconian Alb, Germany). *Facies,* **44**, 1–22.

Arp, G., Bielert, F., Hoffmann, V.W. and **Löffler, T.** (2005) Palaeoenvironmental significance of lacustrine stromatolites of the Arnstadt Formation ("S inm r g k p r", Upp r Tri ssic, N-Germany). *Facies*, **51**, 419-441

Arp, G., Bissett, A., Brinkmann, N., Cousin, S., de Beer, D., Friedl, T., Mohr, K.I., Neu, T.R., Reimer, A., Shiraishi, F., Stackebrandt, E. and **Zippel, B.** (2010) Tufa-forming biofilms of German karstwater streams: microorganisms, exopolymers, hydrochemistry and calcification. In: *Tufas and Speleothems: Unravelling the Microbial and Physical Controls* (Eds M. Pedley and M. Rogerson). *Geol. Soc. London Spec. Publ.,* 336*,* 83–118.

Awramik, S.M. and **Buchheim, H.P.** (2009) A giant, Late Archean lake system: The Meentheena Member (Tumbiana Formation; Fortescue Group), Western Australia. *Precambrian Res.*, **174**, 215-240.

Awramik, S.M. and **Buchheim, H.P.** (2015) Giant stromatolites of the Eocene green river formation (Colorado, USA). *Geology*, **43**, 691–694. Available at: https://doi.org/10.1130/G36793.1

Bahniuk, A.M., Anjos, S., França, A.B., Matsuda, N., Eiler, J., Mckenzie, J.A. and **Vasconcelos, C.** (2015) Development of microbial carbonates in the lower cretaceous codó Formation (north-east Brazil): Implications for interpretation of microbialite facies associations and palaeoenvironmental conditions. *Sedimentology*, **62**, 155-181

Bates, R.L. and **Jackson, J.A., Eds.** (1980) Glossary of Geology, 2nd Edition. Fails Church, American Geological Institute, Virginia, 751 pp.

Bertrand-Sarfati, J., Freytet, P. and **Plaziat, J.C.** (1994) Microstructures in Tertiary nonmarine stromatolites (France). Comparison with Proterozoic, In: *Phanerozoic Stromatolites II* (Eds J. Bertrand-Sarfati and C. Monty), pp. 155–191. Kluwer Academic Publishers, Dordrecht.

Bosak, T., Liang, B., Wu, T.-D, Templer, S.P., Evans, A., Vali, H., Gerquin-Kern, J.L., Klepac-Ceraj, V., Sim, M.S. and **Mui, H.** (2012) Cyanobacterial diversity and activity in modern conical microbialites. *Geobiology,* **10**, 384–401.

Bosak, T., Knoll, A H. and **Petroff, A.P.** (2013a) The Meaning of Stromatolites. *Annu. Rev. Earth Planet. Sci.*, **41**, 21–44. Available at: https://doi.org/10.1146/annurev-earth-042711-105327

Bosak, T., Mariotti, G., Macdonald, F.A., Perron, J.T. and **Pruss, S.B.** (2013b) Microbial sedimentology of stromatolites in Neoproterozoic cap carbonates. *Paleontol. Soc. Pap.*, **19**, 1–25.

Bouton, A., Vennin, E., Boulle, J., Pace, A., Bourillot, R., Thomazo, C., Brayard, A., Désaubliaux, G., Goslar, T., Yokoyama, Y., Dupraz, C. and **Visscher, P.** (2016) Linking the distribution of microbial deposits from the Great Salt Lake (Utah, USA) to tectonic and climatic processes. *Biogeosciences*, **13**, 5511–5526.

Brasier, A.T. Andrews, J.E., Marca-Bell, A.D. and **Dennis, P.F.** (2010) Depositional continuity of seasonally laminated tufas: Implications for $\delta^{18}O$ based palaeotemperatures. *Global Planet. Change*, **71**, 160–167. Available at: https://doi.org/10.1016/j.gloplacha.2009.03.022

Casanova, J. (1986). Les stromatolites continentaux: Paléoecologie, paléohydrologie, paléo-climatologie. Application au Rift Gregory. PhD thesis, Université Marseille-Luminy, Marseille, 256 pp.

Casanova, J. (1994) Stromatolites from the East African Rift: a synopsis. In: *Phanerozoic Stromatolites II* (Eds J. Bertrand-Sarfati and C. Monty), pp. 193–226. Kluwer Academic Publishers, Dordrecht.

Castanier, S., Maurin, A. and **Perthuisot, J.P.** (1989) Production bactérienne expérimentale de corpuscule carbonatés, sphéroïdaux a structure fibro-radiaire, Réflexions sur la définition des ooïdes. *Soc. Géol. Fr. Bul.,* **5**, 589–595.

Chafetz, H.S., Utech, N.M. and **Fitzmaurice, S.P.** (1991) Differences in the $\delta^{18}O$ and $\delta^{13}C$ signatures of seasonal laminae comprising travertine stromatolites. *J. Sed. Petrol.*, **61**, 1015–1028.

Chidsey, T., Vanden Berg, M.D. and **Eby, D.** (2015) Petrography and characterization of microbial carbonates and associated facies from modern Great Salt Lake and Uinta Basin's Eocene Green River Formation in Utah, USA. In: *Microbial Carbonates in Space and Time: Implications for Global Exploration and Production* (Eds D.W.J. Bosence, K.A. Gibbons, D.P. Le Heron, W.A. Morgan, T. Pritchard and B.A. Vining). *Geol. Soc. London Spec. Publ.,* 418, 261–286

Cohen, A.S., Talbot, M.R., Awramik, S.M., Dettman, D.L. and **Abell, P.** (1997) Lake level and paleoenvironmental history of Lake Tanganyika, Africa, as inferred from late Holocene and modern stromatolites. *Geol. Soc. Am. Bull.*, **109**, 444–460. Available at: https://doi.org/10.1130/0016-7606(1997)109<0444:LLAPHO>2.3.CO;2

Craig, H. (1965) The measurement of oxygen isotope palaeotemperatures. In: *Stable Isotopes in Oceanographic Studies and Palaeotemperatures* (Ed. E. Tongiorgi), pp. 161–182. Consiglio Nazionale Della Richerche. Laboratorio de Geologia Nucleare, Pisa.

Decho, A.W., Visscher, P.T. and **Reid, P.** (2005) Production and cycling of natural microbial exopolymers (EPS) within a marine stromatolite. *Palaeogeogr. Palaeoclimatol. Palaeoecol.,* **219**, 71-86.

Deelman, J.C. (1978) Experimental ooids and grapestones: Carbonate aggregates and their origin. *J. Sed. Petrol.*, 48, 503-512.

Della Porta, G. (2015) Carbonate build-ups in lacustrine, hydrothermal and fluvial settings: comparing depositional geometry, fabric types and geochemical signature. In: *Microbial Carbonates in Space and Time: Implications for Global Exploration and Production* (Eds D.W.J. Bosence, K.A. Gibbons, D.P. Le Heron, W.A. Morgan, T. Pritchard and B.A. Vining). *Geol. Soc. London Spec. Publ.,* 418, 17- 68.

Drysdale, R. and **Gillieson, D.** (1997) Micro-erosion meter measurements of travertine deposition rates: A case study from louie creek, Northwest Queensland, Australia. *Earth Surf. Proc. Land*., **22**, 1037–1051.

Duke, W.L. (1985) Hummocky cross-stratification, tropical hurricanes and intense winter storms. *Sedimentology*, **32**, 167–194.

Dumas, S. and **Arnott, R.W.C.** (2006) Origin of hummocky and swaley cross-stratification - The controlling influence of unidirectional current strength and aggradation rate. *Geology*, **34**, 1073–1076. Available at: https://doi.org/10.1130/G22930A.1

Dupraz, C., Pattisina, R. and **Verrecchia, E.P.** (2006) Translation of energy into morphology: Simulation of stromatolite morphospace using a stochastic model. *Sed. Geol.*, **185**, 185-203.

Eyles, N. and **Clark, B.** (1986) Significance of hummocky and swaley cross-stratification in late Pleistocene lacustrine sediments of the Ontario basin, Canada. *Geology*, **14**, 679-682.

Frantz, C.M., Petryshyn, V.A., Marenco, P.J., Tripati, A., Berelson, W.M. and **Corsetti, F.A.** (2014) Dramatic local environmental change during the Early Eocene Climatic Optimum detected using high resolution chemical analyses of Green River Formation stromatolites. *Palaeogeogr. Palaeoclimatol. Palaeoecol.*, **405**, 1–15. Available at: https://doi.org/10.1016/j.palaeo.2014.04.001

Freytet, P. and **Verrecchia, E.P.** (1998) Freshwater organisms that build stromatolites: a synopsis of biocrystallization by prokariotic and eukaryotic algae. *Sedimentology*, **45**, 535-563.

Freytet, P. and **Verrecchia, E.P.** (1999) Calcitic radial palisadic fabric in freshwater stromatolites: diagenetic and recyrstallized feature or physicochemical sinter crust? *Sed. Geol.* **126**, 97-102.

Freytet, P. and **Verrecchia, E.P.** (2002) Lacustrine and palustrine carbonate petrography: An overview. *J. Paleolimnol.*, **27**, 221–237. Available at: https://doi.org/10.1023/A:1014263722766

García-Castellanos, D., Vergés, J., Gasper-Escribano, J. and **Cloetingh, S.** (2003) Interplay between tectonics, climate and fluvial transport during the Cenozoic evolution of the Ebro Basin (NE Iberia). *J. Geophys. Res.*, **108**, 1–18.

Golubic, S. (1973) The relationship between blue-green algae and carbonate deposits. In: *The Biology of Blue-Green Algae* (Eds N.G. Carr and B.A. Whitton), pp. 434-472. Blackwell, Oxford.

Gallois, A., Bosence, D. and **Purgess, P.** (2018) Brackish to hypersaline facies in lacustrine carbonates: Purbeck Limestone Group, Upper Jurassic–Lower Cretaceous, Wessex Basin, Dorset, UK. *Facies*, **64**, 1-39.

Gradzinski, M. (2010) Factors controlling growth of modern tufa: results of a field experiment. *Geol. Soc. London Spec. Publ.*, **336**, 143–191. Available at: https://doi.org/10.1144/SP336.8

Grotzinger, J.P. and **Rothman D.R.** (1996) An abiotic model for stromatolite morphogenesis. *Nature*, **383**, 423-425.

Grotzinger, J.P. and **Knoll, A.H.** (1999) Stromatolites in Precambrian carbonates: Evolutionary Mileposts or Environmental Dipsticks? *Annu. Rev. Earth Panet. Sci.* **27**, 313-358.

Haines, P. (1988) Storm-dominated mixed carbonate/siliciclastic shelf sequence displaying cycles of hummocky cross-stratification, late Proterozoic Wonoka Formation, South Australia. *Sed. Geol.*, **58**, 237-254.

Hand, B.M. and **Bartberger, C.E.** (1988) Leeside sediment fallout patterns and the stability of angular bedforms. *J. Sed. Res.*, **58**, 33–43.

Hofmann, H. J. (1973) Stromatolites: Characteristics and Utility. *Earth-Sci. Rev.*, **9**, 339–373.

Jahnert, R.J. and **Collins, L.B.** (2011) Significance of subtidal microbial deposits in Shark Bay, Australia. *Mar. Geol.*, **286**, 106–111. Available at: https://doi.org/10.1016/j.margeo.2011.05.006

Jahnert, R.J. and **Collins, L.B.** (2013) Controls on microbial activity and tidal flat evolution in Shark Bay, Western Australia. *Sedimentology*, **60**, 1071–1099. Available at:

https://doi.org/10.1111/sed.12023

James, N.P. and **Jones, B.** (2015) Origin of carbonate sedimentary rocks. John Wiley & Sons, Oxford, 464 pp.

Janssen, A., Swennen, R., Podoor, N. and **Keppens, E.** (1999) Biological and diagenetic influence in recent and fossil tufa deposits from Belgium. *Sed. Geol.,* **126**, 75–95. Available at: https://doi.org/10.1016/S0037-0738(99)00033-0.

Jones, B. and **Peng, X.** (2014) Multiphase calcification associated with the atmophytic cyanobacterium Scytonema julianum. *Sed. Geol.*, **313**, 91-104.

Kahle, C.F. (1974) Ooids from Great Salt Lake, Utah, as an analogue for the genesis and diagenesis of ooids in marine limestones. *J. Sed. Petrol.*, **44**, 30- 39.

Kano, A., Hagiwara, R., Kawa, T., Hori, M. and **Matsuoka, J**. (2007) Climatic conditions and hydrological change recorded in a high-resolution stable-isotope profile of a recent laminated tufa on a subtropical island, southern Japan. *J. Sed. Res.*, **77**, 59–67.

Kennard, J.M. and **Burne, R.V.** (1989) Stromatolite Newsletter Number 14. Bureau of Mineral Resources, Geology and Geophisics, Camberra, 179 pp.

Leng, M.J. and **Marshall, J.D.** (2004) Palaeoclimate interpretation of stable isotope data from lake sediment archives. *Quatern. Sci. Rev.,* **23**, 811–831.

Lettéron, A., Hamon, Y., Fournier, F., Séranne, M., Pellenard, P. and **Joseph, P.** (2018) Reconstruction of a saline, lacustrine carbonate system (Priabonian, St-Chaptes Basin, SE France): Depositional models, paleogeographic and paleoclimatic implications. *Sed. Geol.,* **367**, 20–47.

Lindqvist, J.K. (1994) Lacustrine stromatolites and oncoids. Manuherikia Group (Miocene), New Zealand. In: *Phanerozoic Stromatolites II* (Eds J. Bertrand-Sarfati and C.Monty), pp. 227–254. Kluwer Academic Publishers, Dordrecht.

Logan, B.W., Rezak, R. and **Ginsburg, R.N.** (1964) Classification and environmental significance of algal stromatolites. *J. Geol.*, **72**, 68–83. Available at: https://doi.org/10.1086/626965

López-Blanco, C., Andrews, J., Dennis, P., Rosa, M. and **Vicente, E.** (2016) North Atlantic Oscillation recorded in carbonate $\delta^{18}O$ signature from Lagunillo del Tejo (Spain). *Palaeogeogr. Palaeoclimatol. Palaeoecol.*, **441**, 882–889. Available at: https://doi.org/10.1016/j.palaeo.2015.10.037

Manzo, E., Perri, E. and **Tucker, M.E.** (2012) Carbonate deposition in a fluvial tufa system: processes and products (Corvino Valley – southern Italy). *Sedimentology*, **59**, 553–577.

Martin-Bello, L., Arenas Abad, C. and **Alonso-Zarza, A.M.** (2017) Preliminary interpretation of the stable-isotope composition in lacustrine stromatolites of the Sierra de Alcubierre (Miocene, Ebro Basin, Spain). *Geogaceta*, **61**, 171-174.

Matsuoka, J., Kano, A., Oba, T., Watanabe, T., Sakai, S. and **Seto, K.** (2001) Seasonal variation of stable isotopic compositions recorded in a laminated tufa, SW Japan. *Earth Planet. Sci. Lett.*, **192**, 31–44.

Mercedes-Martín, R., Salas, R. and **Arenas, C.** (2014) Microbial-dominated carbonate platforms during the Ladinian rifting: Sequence stratigraphy and evolution of accommodation in a fault-controlled setting (Catalan Coastal Ranges, NE Spain). *Basin Res.*, **26**, 269–296. Available at: https://doi.org/10.1111/bre.12026

Merz-Preiß, M. and **Riding, R.** (1999) Cyanobacterial tufa calcification in two freshwater streams: Ambient environment, chemical thresholds and biological processes. *Sed. Geol.*, **126**, 103–124. Available at: https://doi.org/10.1016/S0037-0738(99)00035-4

Monty, C.L.V. (1976) The origin and development of cryptalgal fabrics. In: *Stromatolites* (Ed. M.R. Walter). *Dev. Sedimentol.,* **20**, 193–249.

, A. and **Villena, J.** (2002) Ebro

Basin (Northeastern Spain). In: *The Geology of Spain* (Eds W. Gibbons and T. Moreno), pp. 301–309, The Geological Society, London.

Muniz, M.C. and **Bosence, D. W. J.** (2015) Pre-salt microbialites from the Campos Basin (offshore Brazil): image log facies, facies model and cyclicity in lacustrine carbonates. In: *Microbial Carbonates in Space and Time: Implications for Global Exploration and Production* (Eds D.W.J. Bosence, K.A. Gibbons, D.P. Le Heron, W.A. Morgan, T. Pritchard and B.A. Vining). *Geol. Soc. London Spec. Publ.,* 418, 221-242.

Nehza, O., Woo, K.S. and **Lee, K.C.** (2009) Combined textural and stable isotopic data as proxies for the mid-Cretaceous paleoclimate: A case study of lacustrine stromatolites in the Gyeongsang Basin, SE Korea. *Sed. Geol.*, **214**, 85-99.

Noffke, N. and **Awramik, S. M.** (2013) Stromatolites and MISS — Differences between relatives. *GSA Today*, **23**, 4–9. Available at: https://doi.org/10.1130/GSATG187A.1.

Okumura, T., Takashima, C., Shiraishi, F., Nishida, S. and **Kano, A.** (2013) Processes forming daily lamination in a microbe-rich travertine under low flow condition at the Nagano-yu Hot Spring, southwestern Japan. *Geomicrobiol J*., **30**, 910–927.

Ordóñez, S., Carballal, R. and **García del Cura, A.** (1980) Carbonatos biogénicos actuales en la cuenca del río Dulce (provincia de Guadalajara). *Bol. Real. Soc. Esp. Hist. Nat. (Geol.)*, **78**, 303–315.

Osácar, C., Arenas, C., Auqué, L., Sancho, C., Pardo, G. and **Vázquez-Urbez, M.** (2016) Discerning the interactions between environmental parameters reflected in $\delta^{13}C$ and $\delta^{18}O$ of recent fluvial tufas: lessons from a Mediterranean climate region. *Sed. Geol.*, **345**, 126-144.

Osácar, M. C., Arenas, C., Vazquez-Urbez, M., Sancho, C., Auque, L. F. and **Pardo, G.** (2013) Environmental Factors Controlling the $\delta^{13}C$ and $\delta^{18}O$ Variations of Recent Fluvial Tufas: A 12-Year Record from the Monasterio de Piedra Natural Park (Ne Iberian Peninsula). *J. Sed. Res.*, **83**, 309–322. Available at: https://doi.org/10.2110/jsr.2013.27

Pardo, G., Arenas, C., González, A., Luzón, A., Muñoz, A., Pérez, A., Pérez-Rivarés, F.J., Vázquez-Urbez, M. and **Villena, J.** (2004) La Cuenca del Ebro. In: *Geología de España* (Ed. J.A. Vera), pp. 533–543. Sociedad Geológica de España-Instituto Geológico y Minero de España, Madrid.

Park, R. (1976) A note on the significance of lamination in stromatolites. *Sedimentology*, **23**, 379–393.

Pedley, H.M., Rogerson, M. and **Middleton, R.** (2009) Freshwater calcite precipitates from in vitro mesocosm flume experiments: a case for biomediation of tufas. *Sedimentology*, **56**, 511–527.

Pentecost, A. (2005) Travertine. Springer-Verlag, Berlin, 445 pp.

Pérez Rivarés, F.J. (2016) Estudio magnetoestratigráfico del Mioceno del sector central de la Cuenca del Ebro: Cronología, correlación y análisis de la ciclicidad sedimentaria. PhD Thesis. University of Zaragoza, Zaragoza, 281 pp.

Pérez-Rivarés, F. J., Garcés, M., Arenas, C. and **Pardo, G.** (2002) Magnetocronología de la sucesión miocena de la Sierra de Alcubierre (sector central de la Cuenca del Ebro). *Rev. Soc. Geol. Esp.*, **15**, 217–231.

Peryt, T.M. (1983) Classification of coated grains. In: *Coated Grains* (Ed. T. M. Peryt), pp. 3–6. Springer, Berlin.

Petryshyn, V. A. and **Corsetti, F.A.** (2011) Analysis of growth directions of columnar stromatolites from Walker Lake, western Nevada. *Geobiology*, **9**, 425–435. Available at: https://doi.org/10.1111/j.1472-4669.2011.00293.x

Petryshyn, V.A., Corsetti, F.A., Berelson, W.M., Beaumont, W. and **Lund, S.P.** (2012) Stromatolite lamination frequency, Walker Lake, Nevada: Implications for stromatolites as biosignatures. *Geology*, **40**, 499–502. Available at: https://doi.org/10.1130/G32675.1

Reid, R.P. and **Browne, K.M.** (1991) Intertidal stromatolites in a fringing Holocene reef complex, Bahamas. *Geology*, **19**, 15–18.

Reid, R.P., James, N.P., Macintyre, I.G., Dupraz, C.P. and **Burne, R.V.** (2003) Shark Bay stromatolites: microfabrics and reinterpretation of origins. *Facies,* **49**, 299–324.

Renaut, R.W., Owen, R., Jones, B., Tiercelin, J.J., Tarits, C., Ego, J.K and **Konhauser, K.O.** (2013) Impact of lake-level changes on the formation of thermogene travertine in continental rifts: Evidence from Lake Bogoria, Kenya Rift Valley. *Sedimentology*, **60**, 428–468. Available at: doi: 10.1111/j.1365-3091.2012.01347.x

Riding, R. (2000) Microbial carbonates: the geological record of calcified bacterial-algal mats and biofilms. *Sedimentology*, **47**, 179–214. Available at: https://doi.org/10.1046/j.1365-3091.2000.00003.x

Riding, R. (2011) Microbialites, stromatolites and thrombolites. In: *Encyclopedia of Geobiology* (Eds J. Reitner and V. Thiel), pp. 635–654. Springer, Heidelberg.

Roche, A., Vennin, E., Bouton, A., Oliver, N., Wattinne, A., Bundeleva, I., Deconinck, J.F., Virgone, A., Gaucher, E.C. and Visscher, P. (2018) Oligo-Miocene lacustrine microbial and matazoan buildups from the Limagne Basin (French Massif Central). *Palaeogeogr. Palaeoclimatol. Palaeoecol.*, **504**, 34-59.

Seong-Joo, L., Browne, K.M. and **Golubic, S.** (2000) On stromatolite lamination. In: *Microbial Sediments* (Eds R.E. Riding, and S.M. Awramik), pp. 16–24. Springer-Verlag, Berlin.

Storrie-Lombardi, M.C. and **Awramik, S.M.** (2006) A sideways view of stromatolites: Complexity metrics for stromatolite laminae. Proc. of SPIE - Instruments, Methods, and Missions for Astrobiology IX, 63090P. Available at: https://doi.org/10.1117/12.679869.

Suarez-Gonzalez, P., Quijada, I.E., Benito, M.I., Mas, R., Merinero, R. and **Riding, R.** (2014) Origin and significance of lamination in Lower Cretaceous stromatolites and proposal for a

quantitative approach. *Sed. Geol.*, **300**, 11–27. Available at: https://doi.org/10.1016/j.sedgeo.2013.11.003

Tang, D., Shi, X. and **Jiang, G.** (2014) Sunspot cycles recorded in Mesoproterozoic carbonate biolaminites. *Precambrian Res.*, **248**, 1–16. Available at: https://doi.org/10.1016/j.precamres.2014.04.009

Tosti, F. and **Riding, R.** (2017) Fine-grained agglutinated elongate columnar stromatolites: Tieling Formation, ca 1420 Ma, North China. *Sedimentology*, **64**, 871–902. Available at: https://doi.org/10.1111/sed.12336

Tucker, M.E. and **Wright,** V.P.(1990) Carbonate sedimentology. Blackwell Science Publications, Oxford, 482 pp.

Vázquez-Urbez, M., Arenas, C., Sancho, C., Osácar, C., Auqué, L. and **Pardo, G.** (2010) Factors controlling present-day tufa dynamics in the Monasterio de Piedra Natural Park (Iberian Range, Spain): depositional environmental settings, sedimentation rates and hydrochemistry. *Int. J. Earth Sci.*, **99**, 1027–1049.

Vazquez-Urbez, M., Arenas, C., Pardo, G. and **Perez-Rivares, J.** (2013) The Effect of Drainage Reorganization and Climate On the Sedimentologic Evolution of Intermontane Lake Systems: The Final Fill Stage of the Tertiary Ebro Basin (Spain). *J. Sed. Res.*, **83**, 562–590. Available at: https://doi.org/10.2110/jsr.2013.47

Vennin, E., Bouton, A., Bourillot, R., Pace, A., Roche, A., Brayard, A., Thomazo, C., Virgone, A., Gaucher, E., Desaubliaux, G. and **Visscher, P.** (2018) The lacustrine microbial carbonate factory of the successive Lake Bonneville and Great Salt Lake, Utah, USA. *Sedimentology*. Available at: doi: 10.1111/sed.12499.

Verrecchia, E.P., Feytet, P., Verrecchia, K. and **Dumont, J.L.** (1995) Spherulites and calcrete laminar crust: biogenico $CaCO_3$ precipitation as major contributor to crust fromation. *J. Sed. Res.*, **A65**, 690–700.

Walter, M.R. (1972) Stromatolites and the biostratigraphy of the Australian Precambrian and Cambrian. *Spec. Pub. Palaeontol.*, **11**, 256.

Woo, K.S., Khim, B.K., Yoon, H.S. and **Lee, K.C.** (2004) Cretaceous lacustrine stromatolites in the Gyeongsang Basin (Korea): Records of cyclic change in paleohydrological condition. *Geosci. J.*, **8**, 179–184. Available at: https://doi.org/10.1007/BF02910193

Zamarreño, I., Anadón, P. and **Utrilla, R.** (1997) Sedimentology and isotopic composition of Upper Palaeocene to Eocene non-marine stromatolites, eastern Ebro Basin, NE Spain. *Sedimentology*, **44**, 159–176.

FIGURE AND TABLE CAPTIONS

Fig. 1. (A) Location of the Ebro Basin in the north-east of the Iberian Peninsula. (B) Geological map of the Sierra de Alcubierre, with the Miocene tectosedimentary units and main lithofacies (compiled from Arenas, 1993 and Arenas & Pardo, 1999). Location of the studied sections is indicated; VS: Valle de Soler; PL: Puig Ladrón; PS: Puig Sabina; AC: Aldea del Correo; LN: Lanaja; SC: San Caprasio; LF: Lasfachastis; BL: Barranco de la Loba.

Fig. 2. Diagram illustrating the three tectosedimentary units in the Sierra de Alcubierre and simplified lateral changes between the different lithostratigraphic units and stromatolite occurrences. Three main facies associations are shown (Facies Associations 1, 2 and 3; modified from Arenas et al., 1997). Lb, Lm, Fg, Fo, St, Ls, Ll, M, Sm, Gn, Glen and Gr refer to facies codes given in Table 1.

Fig. 3. Summarized stratigraphic sections in the Alcubierre Sierra and their correlation (compiled from Arenas, 1993). (A) San Caprasio (SC) and (B) Puig Ladron (PL). Location of sections in Fig. 1B. (C) Detailed section of a portion of the San Caprasio section. Texture and lithology of facies associations: Gy: gypsum; M: mudstone; W: wackestone; P: packstone; G: grainstone; B: boundstone; F: fines; S: sandstones, with fine (Sf), medium (Sm) and coarse (Sm) grain size; G: gravel.

Fig. 4. Field views and thin sections of the main facies in the Sierra de Alcubierre. (A) Succession of laminated limestones with ripples (Ll.1), nodular gypsum (Gn), stromatolitic limestones (Ls) and laminated limestones with ripples (Ll.1). (B) Laminated limestones with ripples and wavy stratification (Ll.1). (C) Alternation of marls (M), with laminated limestones with hummocky cross-stratification (HCS, Ll.2) and parallel lamination (Ll.3). Overlying Ll.3, several layers consisting of massive and bioturbated limestones (Lm and Lb) occur. (D) and (E) Laminated limestones under the optical microscope. (D) Succession consisting of laminated limestones with parallel lamination (Ll.3), massive limestones (Lm), marls (M) and bioturbated limestones (Lb). (E) Succession of laminated limestones with parallel lamination (Ll.3), bioturbated limestones (Lb), stromatolites (Ls) and

laminated limestones with parallel lamination (Ll.3). (F) Succession of bioturbated limestones, stromatolitic limestones (Ls) and laminated limestones with parallel lamination (Ll.3). (G) Alternating intraclast and quartz grain laminae and mudstone laminae. (H) Alternating ooid packstone and mudstone.

Fig. 5. External morphology of the stromatolites based on field observations, their internal growth forms, lamina shape and types of lamina margins in the studied area of the Ebro Basin, based on terms defined in Kennard & Burne (1989).

Fig. 6. External morphologies of the stromatolites and associated carbonate facies based on field observations. (A) Succession of bioturbated limestones (Lb), thin planar stromatolites (Ls.1c), and laminated limestones with parallel lamination (Ll.3). (B) Succession of marls (M), domed stromatolites (Ls.3) and laminated limestones with hummocky cross-stratification (HCS; Ll.2). (C) Plan view of a stratiform stromatolite with circular morphologies from the constituent domes and columns from a stratiform stromatolite (Ls.2). (D) Alternation of thin planar stromatolites (Ls.1a, Ls.1b) with laminated limestones consisting of HCS (Ll.2). Some of the stromatolites are covering erosional surfaces (red dashed line). Laminated limestones with parallel lamination (Ll.3) at the top. (E) Succession of marls (M), alternating intraclastic limestone (Ll.1) and thin planar stromatolites (Ls.1a), stratiform stromatolite (Ls.2) and laminated limestones with parallel lamination (Ll.3).

Fig. 7. Internal growth forms visible in polished sections (A) to (G) and field view (H) showing varied geometry of stromatolites, oncolites and associated facies. (A) Oncolite (Lo). (B) Thin planar stromatolites (Ls.1a) and overlying laminated limestones with parallel lamination (Ll.3). (C) Thin planar stromatolites (Ls.1b). (D) Succession of bioturbated limestones (Lb), thin planar stromatolites (Ls.1b) and laminated limestones (Ll.1 and Ll.3). Note fragments of facies Lb within Ll.3. (E) Thin planar stromatolites (Ls.1c) that developed on an intraclasts packstone-rudstone layer (Ll.1). (F) Portion of a domed stromatolite (Ls.3). (G) Portion of a stratiform stromatolite (Ls.2). (H) Field close-up view of a stratiform stromatolite (Ls.2).

Fig. 8. Facies associations (FA) that include the different types of stromatolites in the Sierra de Alcubierre. Four variants from carbonate FA2 in Fig. 2 (FA2-A, FA2-B, FA2-C and FA2-D), modified from Martin-Bello et al. (2016). Texture and lithology of facies associations: Gy: gypsum; M: mudstone; W: wackestone; P: packstone; G: grainstone; B: boundstone; F: fines; S: sandstones, with fine (Sf), medium (Sm) and coarse (Sm) grain size; G: gravel. Colours and facies codes refer to Table 1.

Fig. 9. The concepts of simple and composite laminae in stromatolites based on thin sections of the Sierra de Alcubierre. (A) Dark dense (DD, red arrow) and light porous simple laminae (LP, blue arrows). (B) Alternation of dark composite laminae (DCL) and light composite laminae (LCL). Light composite laminae are formed of light porous (LP) laminae (blue arrow) with thin dark dense (DD) simple lamina intercalations (red arrow). Each group of dominant dark dense simple laminae forms a dark composite lamina.

Fig. 10. Photomicrographs (optical microscope) of the diverse types of stromatolite laminae and lamination. (A) Micritic stromatolite with light dense (LD), light porous (LP) and dark dense laminae forming dark composite laminae (DCL) in a conical morphology. (B) Stromatolite constituted by dark dense and light porous simple laminae combined in different lamination patterns as for example dark composite laminae (DCL) followed by light composite laminae LCL (Type C; Fig. 10). (C) Detail of (B) showing dark dense laminae (DD) and light porous and microsparite laminae (LD). (D) Stromatolite including fibrous laminae (white arrows), porous laminae (LP), light dense micrite laminae (LD) with ooids and dark composite laminae (DCL). (E) Stromatolite including fibrous laminae changing laterally to dark dense laminae. (F) Micritic stromatolite consisting of alternating light dense micrite (LD) and light porous/clotted micrite to microsparite (LP) laminae forming a light composite laminae (LCL), with dark composite laminae (DCL) towards the top (Type C; Fig. 10). (G) Micritic stromatolite consisting of dark composite laminae (DCL) at the base, light porous micrite to

microsparite laminae (LP), light dense micrite laminae (LD) and dark dense laminae (DD) (Type C; Fig. 10). (H) Fibrous laminae with the crystal long axes perpendicular to the lamination.

Fig. 11. Types of laminae (A) and (B) and lamination patterns (C) to (H) in micritic stromatolites. (A) Simple laminae: dark dense micrite (DD), light porous/clotted micrite to microsparite (LP), light dense micrite (LD) and fibrous laminae. (B) Dark composite laminae (DCL). DC1: dark dense micrite laminae that alternate with thinner light porous/clotted micrite to microsparite laminae. DC2: successive dark dense micrite laminae. Light composite laminae (LCL). LC1: thick light porous/clotted micrite to microsparite lamina with thin dark dense micrite, simple lamina intercalations. LC2: alternation of light porous/clotted micrite to microsparite laminae and light dense micrite laminae. (C) Three types of lamination patterns in the micritic stromatolites exemplified by images (D) to (H).

Fig. 12. Microbial evidence. (A) Palisade of filamentous bodies (red arrows) set perpendicular to lamination. (B) Elongate shapes (sub)perpendicular to lamination that consist of dense micrite (red arrows). (C) Domed or fan-like shapes in a light porous/clotted micrite to microsparite lamina, delineated at the top by a dark dense micrite lamina (red arrows).

Fig. 13. (A) Cross-section of the upper part of a thin planar stromatolite and the correspondent stable isotopic profile. (B) Cross-section of the lower part of the same thin planar stromatolite and the correspondent stable isotopic profile. Samples belongs to unit T6 in section SC. In some cases, one value represents the average of several samples. l: light laminae; d: dark laminae (data compiled from Martin-Bello et al., 2017).

Fig. 14. Conceptual facies model for Miocene stromatolite formation in the Sierra de Alcubierre (not to scale): (A), (B) and (C) correspond to intermediate lake water levels (WL2, saline carbonates) between high water level (WL1, freshwater carbonates, facies Lm, Lb) and low lake level (sulphate precipitation, not shown in the figure). (A) and (C) Fair-weather conditions, with stromatolite (Ls) and

laminated limestones (Ll.1) formation. Note that previous high water lake level (WL1) led to massive and bioturbated facies formation in freshwater (Lm and Lb). During WL2, the deposition areas with Lm and Lb became exposed and underwent desiccation, brecciation and other subaerial processes (i.e. channel incision). (B) Storm conditions, with formation of hummocky cross-stratification (Ll.2) and breakage of stromatolites.

Fig. 15. Examples of discontinuous stromatolite internal growth forms associated with laminated limestones (Ll) and erosion phases. Polished samples from sections SC [(A) and (B); unit T6] and VS [(C) and (D; unit T5]. In (B) and (D), numbers correspond to stromatolite phases and letters to facies Ll. Note in (A) and (B) the irregular surface of phase E, clearly produced by erosion of facies Ll.1 deposits, later coated by stromatolites Ls.1 (phase 4), with highly enveloping laminae. Note in (C) and (D) the occurrence of intraclasts deposits between columns, and the enveloping character of the stromatolite laminae.

Fig. 16. (A) Variations of stromatolite lamina shape, lamina continuity and internal growth forms as a function of water depth, energy and sediment supply. (B) Summary of the factors that control the external geometry and internal structure of stromatolites.

Fig. 17. Summary of textural types of laminae and lamination patterns as a function of the Precipitation/Evaporation rate (P/E) and time elapsed (T).

Table 1. Textural and structural features, and depositional interpretation of the different facies, summarized from Arenas et al. (1997, 2007).

Table 2. Mineralogy and stable isotope values of the different facies and subfacies in the studied tectosedimentary units (TSU). Mineralogical percentages are semi-quantitative estimates from XRD of calcite, dolomite, aragonite, quartz and feldspar, clay minerals and calcium sulphates. The stable isotope values (‰ VPDB) are compiled from: (1) Arenas & Pardo (1999) (parenthesized values), and (2) Martin-Bello et al. (2017).

Table S1. $\delta^{13}C$ and $\delta^{18}O$ values of successive laminae in three stromatolite specimens. SC-31p: unit T6, section SC; SC-141: unit T6, section SC; VS-22: unit T5 in section VS.

Facies and subfacies		Figures	Texture and components	Sedimentary structures	Interpretation
Bioturbated limestones: Lb		4C, 4D, 4E, 4F, 6A and 7B	Mudstones and wackestones. Gastropods, ostracods and charophytes	Bioturbation (root traces), desiccation cracks, nodules and breccias	Palustrine conditions; shallowing of previous fresh water ponded areas
Massive limestones: Lm		4C and 4H	Mudstones and wackestones. Gastropods, ostracods and charophytes	Structureless, non-laminated. If present, weak bioturbation (root traces)	Freshwater, shallow lacustrine areas. Permanent water supply
Laminated limestones: Ll	Ll.1	4A, 4B, 7C and 7D	Micrite and dolomicrite with millimetre to centimetre detrital laminae and lenses. Detritals include quartz, intraclasts, coated grains, ooids and bioclasts. Carbonate grains commonly form packstones and rare rudstones. Silicate grains constitute very fine to coarse sandstones	Lenticular or wavy stratification	Wave action during fair-weather conditions, above storm-surge level
	Ll.2	4C, 6B and 6D		Hummocky cross-stratification	Dominant storm-surge action below fair-weather wave level
	Ll.3	4C, 4D, 4E, 4F, 4G, 4H, 6A, 6D, 6E, 7B and 7D		Parallel lamination	Shore sheet flows or inner turbidite-like currents offshore
Marls: M		4C, 6B and 6E	Fine siliciclastic (clays and silts) sediment and lime mud. Gastropods, ostracods, charophytes and bioturbation	Structureless or with horizontal lamination or lenticular stratification	Settle-out of fine sediment in offshore lake areas in relation to water inputs
Stromatolitic limestones: Ls	Ls. 1	4A, 6A, 6D, 6E, 7B, 7C and 7D	Boundstones. Lamination composed of simple laminae: dark dense micrite, light porous micrite to microsparite, and light dense micrite; combined in composite dark and light laminae	Thin planar stromatolites	Microbial growth structures in shallow/marginal lacustrine areas. Moderate salinity waters and varying water depth and surge action
	Ls. 2	6E and 7F		Stratiform stromatolite	
	Ls. 3	6B, 7G and 7H		Domed stromatolite	
Oncolitic limestones: Lo		7A		Oncolites	
Mudstones: Fg and Fo		–	Siliciclastic sediment (clays and silts)	Green, grey and ochre. Structureless or parallel lamination	Nearshore lake areas or alluvial plains surrounding lacustrine areas. Locally deltaic deposits
Sandstones: Sm, Sr and St		–	Siliciclastic sand-size sediment	Massive, rippled and trough cross-stratification	Sheet flows and channels of alluvial plain near or within the lake areas.
Nodular gypsum: Gn		4A	Alabastrine, saccharoid	Nodules, grouped in beds or isolated within previous deposits	Evaporative processes in saline mud flats
Lenticular gypsum: Glen		–	Alabastrine, saccharoid	Lenticular bedding and rarely forming laminae	Gypsum precipitation in water lake and interstitial within the sediment
Rippled & Laminated gypsum: Gr and Gl		–	Alabastrine, saccharoid	Parallel and rippled lamination, and lenticular bedding	Gypsum precipitation in hypersaline lake water

Facies and subfacies	TSU	Nº	Calcite $\delta^{13}C$ (‰VPDB)	Calcite $\delta^{18}O$ (‰VPDB)	Calcite %	Dolomite %	Aragonite %	Quartz + feldspar %	Clay minerals %	Calcium sulphates %
Bioturbated limestones: Lb	5	4	-2.5 ±0.9	-5.6 ±0.6	93.9 ±5.3	0	0	6.1 ±5.3	0	0
		(17)	(-3.1 ±1.4)	(-6.1 ±0.9)	(95.8 ±2.9)	(0.2 ±0.6)	–	(2.8 ±1.6)	(1.2 ±1.6)	–
Bioclastic massive limestones: Lm		3	-1.6 ±0.2	-4.8 ±3.3	97.7 ±1.5	0	0	2.3 ±1.5	0	0
		(10)	(-2.6 ± 2.6)	(-6.1 ±1.2)	(92.0 ±10.0)	(0)	–	(5.3 ±6.0)	(2.7 ±4.3)	–
Laminated limestones: Ll		18	-1.3 ±0.7	-2.8 ±2.0	67.4 ±26.4	18.5 ±24.5	2.0 ±5.7	8.7 ±5.5	1.1 ±2.9	0.1 ±0.9
		(47)	(-1.9 ±0.9)	(-2.9 ±2.7)	(68.7 ±32.7)	(20.6 ±33.1)	–	(5.9 ±3.7)	(4.8 ±3.8)	–
Marls: M		4	-1.5 ±1.3	-3.5 ±3.3	34.8 ±24.7	18.2 ±29.1	6.5 ±10.6	20.2 ±10.9	6.6 ±10.5	0
		(4)	(-3.0 ±0.7)	(-4.6 ±0.9)	(42.3 ±9.7)	(4.0 ±8.0)	–	(22.0 ±6.0)	(31.8 ±5.4)	–
Stromatolitic and oncolitic limestones: Ls and Lo	5 & 6	20	-1.2 ±0.4	-3.5 ±1.5	79.9 ±22.9	14.3 ±22.6	0	2.7 ±3.3	0.1 ±1.0	1.2 ±4.4
		(59)	(1.7 ±1.2)	(-3.2 ±2.6)	(84.8 ±25.9)	(15.8 ±31.5)	–	(2.8 ±1.6)	(1.2 ±1.9)	–

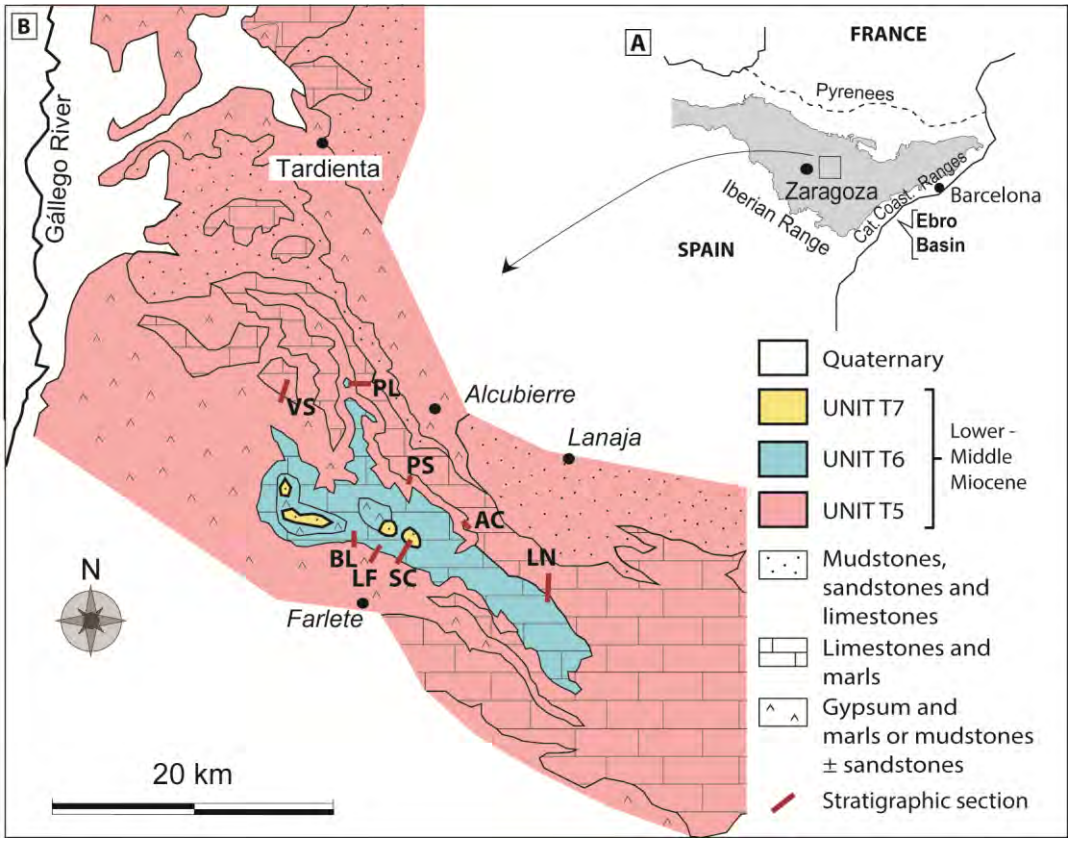

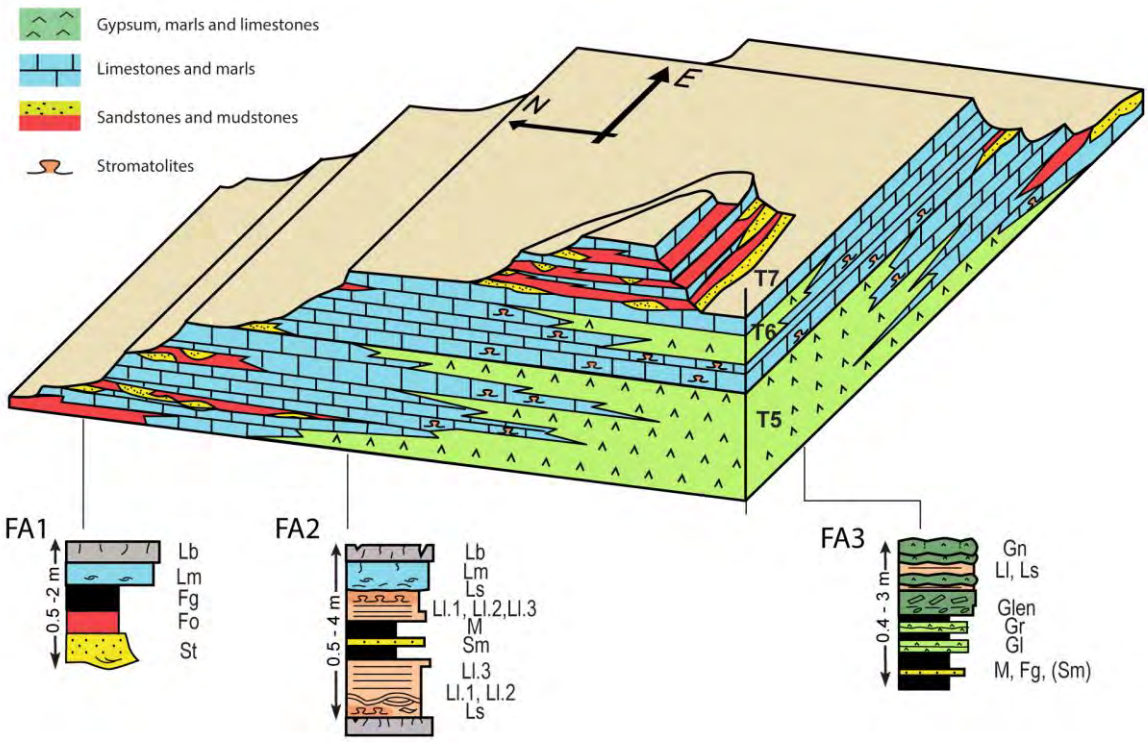

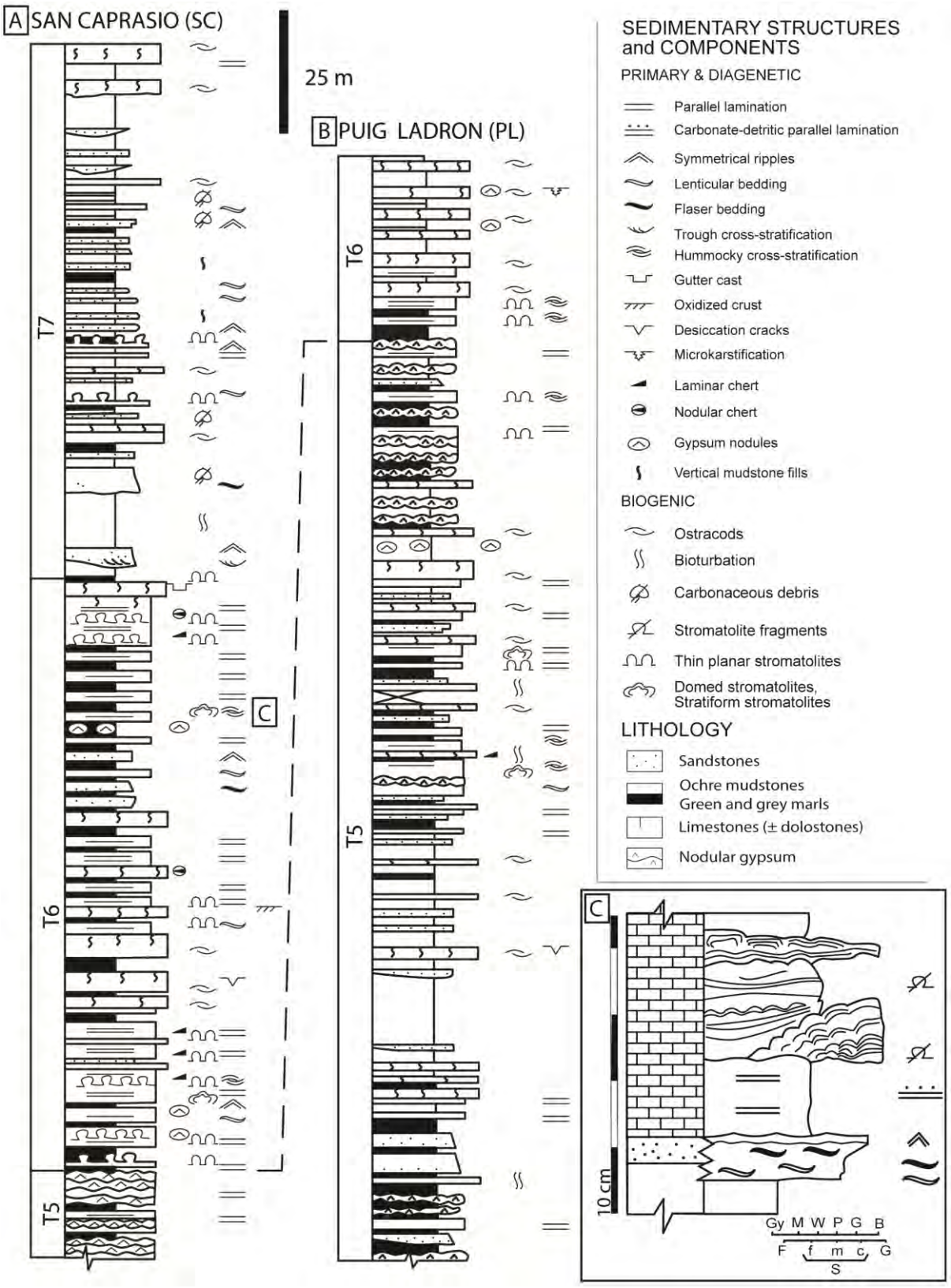

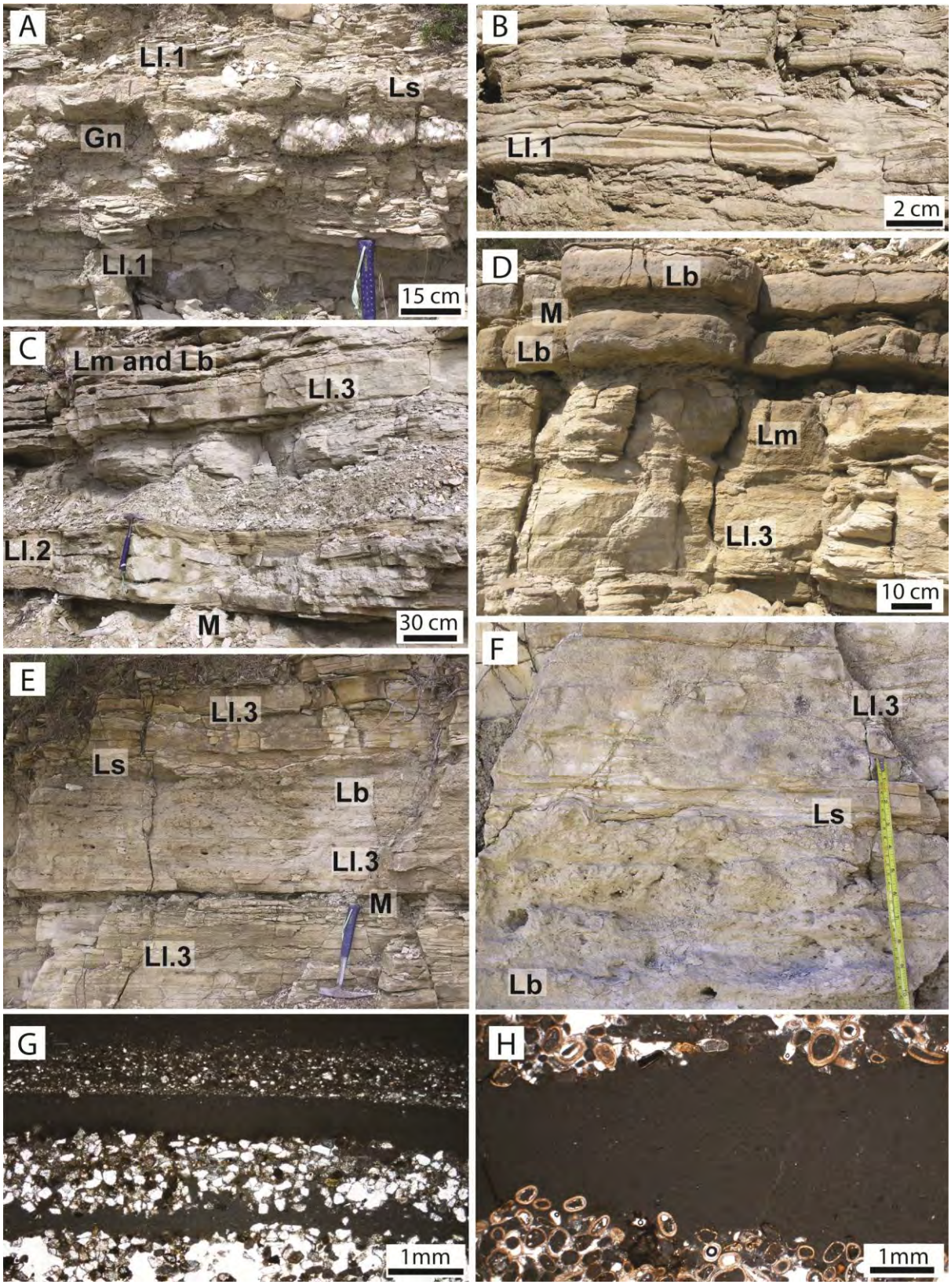

External morphology of the stromatolites based on field observations

Internal growth forms of the stromatolites

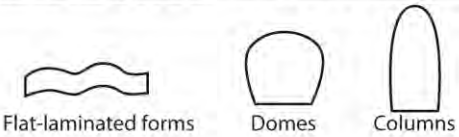

Lamina shape

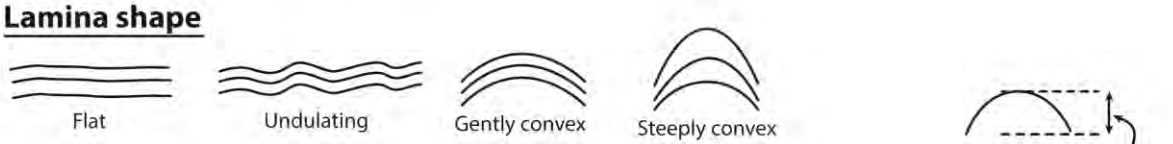

Types of lamina margins